ELUCIDATION OF THE MECHANISM OF ACTION OF A CELL LINE SELECTIVE TOXIN

APPROVED BY SUPERVISORY COMMITTEE:

_____
Deepak Nijhawan, M.D., Ph.D.

_____
Hongtao Yu, Ph.D.

_____
Michael S. Brown, M.D.

_____
Zhijian J. Chen, Ph.D.

_____
Joseph M. Ready, Ph.D.

DEDICATION

I would like to thank my mentor, Dr. Deepak Nijhawan, for his significant investment of time and effort in my training. With his guidance I have continued to view science as an incredibly worthwhile and enjoyable endeavor and I have gained respect for the rigorous practice of the scientific method. I would like to thank Dr. Steven L. McKnight who, early on in my PhD, reignited the passion for discovery I had as a child, introduced me to my mentor and provided guidance throughout my training. Together, the above two scientists have taught me how to choose and approach scientific problems of interest. I would especially like to thank Dr. Joe Ready, Dr. Noelle Williams and members of their labs who contributed substantially to the following work. I would like to thank my thesis committee, members of the Nijhawan lab, the McKnight lab, the Brown and Goldstein lab, the Williams lab, the Ready lab, the Tu lab and the Medical Scientist Training Program for providing valuable advice and the infrastructure for my work. Finally, I would like to thank my family for its continuous support and encouragement during my PhD training.

ELUCIDATION OF THE MECHANISM OF ACTION OF A CELL LINE SELECTIVE TOXIN

by

PANAYOTIS C. THEODOROPOULOS

DISSERTATION

Presented to the Faculty of Graduate School of Biomedical Sciences

The University of Texas Southwestern Medical Center at Dallas

In Partial Fulfillment of the Requirements

For the Degree of

DOCTOR OF PHILOSOPHY

The University of Texas Southwestern Medical Center at Dallas

Dallas, Texas

May 3, 2019

ELUCIDATION OF THE MECHANISM OF ACTION OF A CELL LINE SELECTIVE TOXIN

Publication No. _____

Panayotis C. Theodoropoulos

The University of Texas Southwestern Medical Center at Dallas, 2015

Supervising Professor: Deepak Nijhawan, MD, PhD

Abstract: A hallmark of targeted cancer therapies is selective toxicity among cancer cell lines. We evaluated results from a viability screen of over 200,000 small molecules to identify two chemical series, oxalamides and benzothiazoles, that were selectively toxic to the same four of 12 lung cancer cell lines at low nanomolar concentrations. Sensitive cell lines expressed cytochrome P450 (CYP) 4F11, which metabolized the compounds into irreversible stearoyl CoA desaturase (SCD) inhibitors. SCD has been recognized as a promising biological target in cancer and metabolic disease. However, SCD is essential to sebocytes, and accordingly SCD inhibitors cause skin toxicity. Mouse sebocytes were unable to activate the benzothiazoles or oxalamides into SCD inhibitors, providing a therapeutic window for inhibiting SCD *in vivo*. We thus offer a strategy to target SCD in cancer by taking advantage of high CYP expression in a subset of tumors.

TABLE OF CONTENTS

PUBLICATION PRESENTED IN THIS DISSERTATION

Panayotis C. Theodoropoulos[†], Stephen S. Gonzales[†], Sarah E. Winterton, Carlos Rodriguez-Navas, John S. McKnight, Lorraine K. Morlock, Amy E. Owen, Yingli Duan, Jose R. Moreno, Jordan M. Hanson, Bethany Cross, Andrew Lemoff, Hamid Mirzaei, Bruce A. Posner, Noelle S. Williams, Joseph M. Ready*, Deepak Nijhawan*. *Nat. Chem. Biol. (In press).* [†] and * equal contribution.

Author Contributions

P.C.T., designed and performed target identification, compound selectivity and compound toxicity studies; S.S.G., synthesized all of the benzothiazoles in the optimization that led to SW203668, Xenon-45, Alexa Fluor dye azide, and dMe-SW208108; S.E.W., synthesized all of the oxalamides in the optimization that led to SW208108; C.R.N., performed fatty acid flux analysis; J.S.M., performed molecular cloning; L.K.M., J.M.H. and B.C., performed pharmacokinetic and compound metabolism studies; A.E.O. and Y.D., assisted with compound concentration response studies; J.R.M., synthesized SW209049; A.L. and H.M., performed protein mass spectrometry; B.A.P., developed and used the S-Score analysis to identify potential selective toxins and performed unsupervised hierarchical clustering; N.S.W., designed, performed and supervised xenograft, pharmocokinetic, compound metabolism and compound toxicity studies; J.M.R., designed and supervised chemical synthetic strategies, target identification and compound toxicity studies; D.N. designed and supervised target identification, compound selectivity and compound toxicity studies.

LIST OF FIGURES AND TABLES

Figure 6-1: The CYP-activated SCD inhibitors are not activated by sebaceous glands and display a therapeutic window to avoid sebaceous gland toxicity compared to known SCD inhibitors.

Figure 6-2: Supplementary information for figure 6-1.

Table 4: Data collected from cbioportal.org summarizing CYP over-expression in human tumors (figure 6-1e).

LIST OF SUPPLEMENTARY DATASETS

Supplementary Dataset 1: List of toxins from high throughput small molecule screen on a panel of 12 non-small cell lung cancer cell lines.

Supplementary Dataset 2: List of S-score small molecule hits.

Supplementary Dataset 3: Mass spectrometry list of proteins pulled down in the purification of p37 and p30.

Supplementary Chemical Procedures: Methods for chemical synthesis of small molecules presented in the following work.

Introduction

The ideal medical treatments for cancer achieve a therapeutic index by exploiting differences between cancerous and normal cells. Cancers acquire genetic and genomic alterations and, as a consequence, aberrantly express many proteins compared to normal cells[1]. Therapies that target these differences exhibit a high therapeutic index because they are not universally toxic but instead selectively impede the proliferation of cells having a cancer-specific genotype. For example, erlotinib and crizotinib, which are targeted drugs for the treatment of lung cancer, are most effective in cancers that harbor either *EGFR* mutations or *EML4-ALK* translocations, respectively[2-4]. Therefore, an objective in cancer drug discovery is to match cancer genotypes with specific chemical vulnerabilities.

Compared to normal cells, many cancers express higher levels of cytochrome P450 (CYP) mixed function oxidases[5]. Amongst other functions, these enzymes metabolize xenobiotics[6]. The reason for high CYP expression in cancers is not known. One possibility is that increased CYP expression might activate pro-carcinogens, thus promoting transformation[5]. Alternatively, the altered expression pattern of P450 enzymes might be a by-product of extensive genomic alterations. A potential strategy to target toxins to cancer takes advantage of elevated CYP expression by delivering pro-drugs that are locally bio-activated into toxins within the tumor[7]. In other cases, adenoviral vectors have been used to deliver CYP enzymes to tumors in order to activate the anti-tumor drug cyclophosphamide[8].

This mechanism of targeting has the advantage of locally producing and potentially concentrating the active drug within the tumor, and may represent a general strategy to achieve favorable therapeutic indices for cancer treatments.

Non-small cell lung cancers express CYP mixed function oxidases, including CYP4B1[9]. CYP4B1 can locally activate the molecule 4-ipomeanol into a reactive species that is able to alkylate numerous proteins, as well as DNA, leading to cell death[7,10]. However, CYP4B1 is also expressed in the liver. Not surprisingly, activation of 4-ipomeanol by CYP4B1 in the liver causes hepatotoxicity[9], which limits the potential of 4-ipomeanol as a targeted treatment for cancer. Thus, the high expression of multiple CYP enzymes in the liver presents a potential obstacle for the development of bio-activated toxins. Accordingly, bio-activated metabolites of the pro-drug need to be toxic to the tumor but not to the liver.

Here we present a strategy for the development of CYP-activated inhibitors of stearoyl CoA desaturase (SCD). SCD is an enzyme of the endoplasmic reticulum, which performs the first step in the *de novo* synthesis of unsaturated fatty acids by inserting a double bond in the Δ9 position of saturated fatty acids. Importantly, SCD is not essential in the liver. Mice with liver-specific deletion of the major isoform of SCD have no observed abnormalities[11]. Furthermore, no significant toxicity was reported in a Phase II trial of a compound that utilizes organic anion transporters to concentrate SCD inhibitors in the livers of human patients[12]. In contrast, SCD is an effective target for cancer cells because they are often in a nutrient poor environment and by virtue of their need to generate biomass require *de novo* synthesized unsaturated fatty acids to synthesize membranes, maintain membrane

fluidity, and buffer the cell from the toxic effects of saturated fatty acids and free cholesterol[13-15]. Indeed, small molecules that inhibit SCD are toxic to cancer cell lines, both in culture as well as in xenograft-derived cancer models in mice[16-19].

The clinical potential of known SCD inhibitors has been limited by mechanism-related toxicity[20,21]. Specifically, mice dosed with these inhibitors suffer atrophy of sebocytes. Mouse sebocytes require SCD to synthesize sebum, which is composed of esters of fatty acids and fatty alcohols. Sebum is secreted into the urine by the preputial gland to mark territory, onto the skin by the hair follicles to reduce heat loss, and onto the eye and eyelid by the meibomian gland for lubrication[22]. As a result, mice treated with these inhibitors have dry eye and dry skin, which leads to cold-induced hypothermia[20,21]. Accordingly, an effective SCD inhibitor for cancer therapy would need to block enzymatic function within the tumor while sparing SCD activity in sebocytes.

Using a small molecule screen of lung cancer cell lines we identified two chemical scaffolds that are selectively toxic to a subset of cell lines derived from non-small cell lung cancer (NSCLC). We discovered that their selectivity was explained by differential expression of CYP4F11, which activates the compounds into potent and irreversible SCD-specific inhibitors.

Chapter 1: Small molecule screen reveals selective toxins, the benzothiazoles and oxalamides, both of which target 37kDa and 30kDa proteins

The UT Southwestern Center in the Cancer Target Discovery and Development Network (CTD2) screened over 200,000 compounds at a concentration of 2.5 μM on 12 different NSCLC cell lines and identified 15,483 candidate cancer toxins (Supplementary Dataset 1)[23,24]. We assigned a score to each compound in order to identify candidate selective toxins (Fig. 1-2a). Specifically, for each compound, we ranked the cell lines from most to least sensitive, and then divided them sequentially into 11 sets of two groups, designated *Sensitive* and *Resistant* (Fig. 1-2b). For each set, we then calculated the difference in viability (Δ_{1-11}) between the $Sensitive_{min}$ (the least sensitive cell line in the group) and $Resistant_{max}$ (the most sensitive cell line in the group). The maximum Δ_n was assigned to each compound as the selectivity score or "S-Score". The distribution of small molecule S-Scores had two peaks (Fig. 1-2c). The first peak represented compounds that were either universally toxic or non-toxic and, therefore, exhibited little variance in toxicity between cell lines. The second peak represented a skew normal distribution. We arbitrarily selected the 1,047 small molecules with S-Scores greater than 40, which represented the top 6.7% of compounds. To minimize further investigation of compounds that might be toxic to non-cancerous cells, we eliminated 499 compounds that decreased the viability of HBEC30KT[24] by more than 20% (see highlighted rows in Supplementary Dataset 1). In addition, we

removed 28 compounds because there was a high degree of variance amongst the biological replicates for the sensitive cell lines[23].

Unsupervised, hierarchical clustering of the activities of the remaining 520 compounds revealed groups of small molecules with similar selectivity profiles (Fig. 1-2d). Interestingly, the toxicity profile of two small molecule scaffolds clustered together in spite of chemical differences (Fig. 1-2e, see highlighted rows in Supplementary Dataset 2). One scaffold, represented by 17 compounds, contained an acylated amino-benzothiazole, hereafter referred to as the benzothiazole. The other scaffold, represented by four compounds, contained an oxalic acid diamide moiety, hereafter referred to as the oxalamide.

To validate the selective toxicity of these compounds, we tested representative oxalamide SW027951 (**1**) and benzothiazole SW001286 (**2**) compounds (Fig. 1-2f) for toxicity in the same 12 cancer cell lines using a concentration response study ranging from 0.3 nM to 6 μM (Fig. 1-2g). For the oxalamide and the benzothiazole, the concentration that resulted in 50% less viability (IC_{50}) was less than 0.1 μM for both the H2122 and H460 cell lines. Eight of the remaining ten cell lines were insensitive to 6 μM of either compound and in two cell lines, HCC44 and HCC95, the small molecules showed intermediate toxicity. The fact that both scaffolds were toxic to the same cell lines raised the hypothesis that both compounds, in spite of their chemical differences, either affect the same pathway or share the same biological target.

To enhance the potency of these compounds while retaining cancer cell line selectivity, we synthesized approximately 100 benzothiazoles and 200 oxalamides

and analyzed their activity across a subset of the lung cancer cell lines (full medicinal chemistry analysis to be published elsewhere). The medicinal chemistry optimization resulted in two lead molecules (Fig. 1a, Fig. 1-2f). The optimized oxalamide, SW208108 (**3**), was toxic to four cell lines (IC_{50} 0.014 μM to 0.031 μM), intermediately toxic to one cell line (H2073, IC_{50} ~0.69 μM) and non-toxic to seven other cell lines (IC_{50} > 10 μM) (Fig 1a, b). The optimized benzothiazole, SW203668 (**4**), was selectively toxic to the same four cell lines (IC_{50} 0.022 μM to 0.116 μM) and non-toxic to the eight other cell lines (IC_{50} > 10 μM) (Fig 1a, b). We were unable to to formulate oxalamides for *in vivo* administration due to poor solubility (Table 1). Further, benzothiazoles were stable in S9 extract, a marker for predicted bioavailability (Table 1). A pharmacokinetic analysis of SW203668 revealed plasma levels that exceeded 0.3 μM (~14-fold above the *in vitro* IC_{50}) for the first six hours and a half-life of eight hours after an intraperitoneal (IP) injection of 25 mg compound/kg body weight (Fig. 1-2h).

We treated immune-deficient mice bearing 200 mm^3 tumors derived either from H2122 cells (sensitive, IC_{50} 0.022 μM) or H1155 cells (insensitive, IC_{50} > 10 μM) with 25 mg/kg of SW203668 delivered by IP injection twice a day for 10–15 days (Fig. 1-2i). After the compound was administered, we observed a significantly reduced rate of growth in H2122 derived tumors. The H1155 derived tumors were unaffected, providing evidence that the selectivity and cytotoxicity of SW203668 are maintained *in vivo*.

The optimized oxalamide, SW208108, although unsuitable for *in vivo* studies, was ideally suited for target identification. SW208108 contains a benzophenone,

which can be cross-linked to binding partners following activation by UV light. It also features an alkyne, which facilitates conjugation by copper-assisted [3+2] cycloaddition between the alkyne and azide moieties of a fluorescent dye or biotin, hereafter referred to as click chemistry[25]. Thus, we cultured sensitive (H2122) cells (SW208108 IC_{50} = 0.014 μM) in the presence of varying concentrations of SW208108 with or without exposure to ultraviolet (UV) radiation. We then subjected the resulting protein lysates to a copper-dependent click reaction in the presence of a fluorescent dye-azide conjugate. Compound-bound proteins were separated by SDS-PAGE and analyzed using a fluorescence imager. In this way, we were able to analyze both covalent (UV independent) and non-covalent (UV dependent) binding partners for SW208108.

In the absence of UV radiation, SW208108 cross-linked to proteins that migrated at both 37kDa (p37) and 30kDa (p30), reflective of covalent modification (Fig. 1-1c). This cross-linking was evident at 0.01 μM, which is consistent with the IC_{50} of the compound in cellular toxicity assays. Of note, we observed multiple UV dependent bands at concentrations that exceeded the IC_{50} of the probe, which suggested non-specific interactions. To determine the functional relevance of p37 and p30, we performed competition experiments wherein we co-incubated SW208108 with 10-fold excess of different oxalamide analogues representing a range of potencies. Active analogues specifically decreased the intensity of both bands, while less active ones did not (Fig. 1-1d). This correlation between cytotoxic activity and binding supported the hypothesis that p37 and p30 represent the biological targets for oxalamide toxicity.

The competition assay indicated that benzothiazoles also bind p37 and p30. Most strikingly, the less toxic enantiomer, (+)-SW203668 (**5**) (0.029 μM) competed for binding 6-fold less effectively than the more toxic enantiomer (–)-SW203668 (**6**) (0.007 μM, Fig. 1-1e, Fig. 1-2j). We expanded this analysis by measuring binding of a panel of 30 oxalamide and benzothiazole analogues to p37 and p30. Binding to both p37 and p30 correlated with the activity of the compound with an R^2 value of 0.87 and 0.83, respectively (Fig. 1-1g, Fig. 1-2k, Table 2). Moreover, the EC_{50} of the p37 correlation curve was 0.31 μM, which was approximately 10-fold the IC_{50} of SW208108, consistent with our experimental conditions of a 10-fold excess of competitor. Finally, we used an alkyne-containing benzothiazole, SW209049 (**7**) (H2122 IC_{50} = 0.29 μM) to confirm that the benzothizoles also covalently modify p37 and p30 (Fig. 1-2l, m). Taken together, these results suggested that the benzothiazoles and oxalamides both act through the same target.

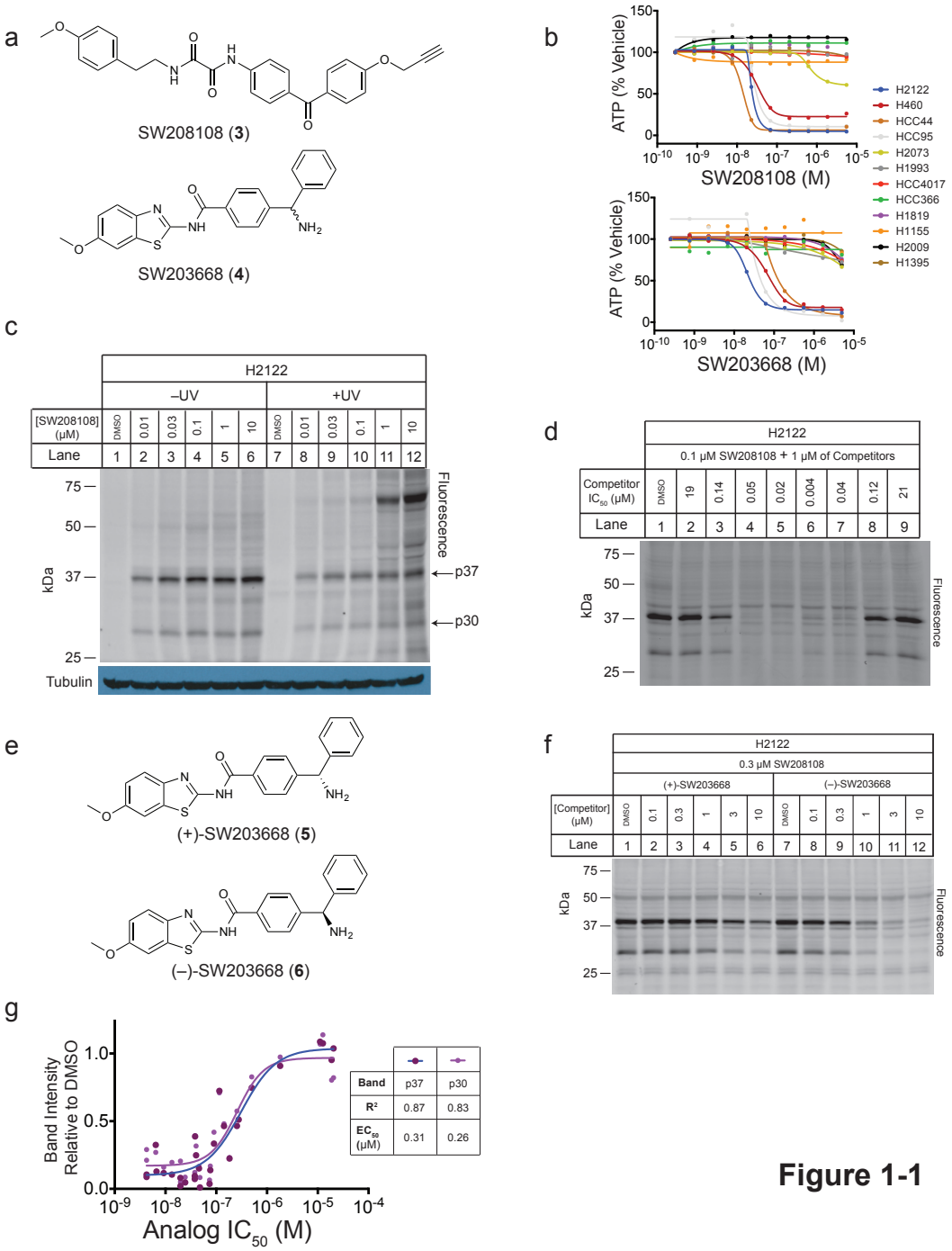

Figure 1-1

Figure 1-1: Oxalamides and benzothiazoles are selective toxins identified in a high throughput small molecule phenotypic screen that target the same proteins.

Legend for Figure 1-1. a. Chemical structures of the optimized oxalamide probe, SW208108, and the optimized bioavailable benzothiazole, SW203668. b. Concentration-response toxicity curves across a panel of 12 NSCLC cell lines. Each point represents the average of two biological replicates. c. SW208108 cross-linking to proteins in H2122, a sensitive cell line. Lysates were clicked to Alexafluor 532-azide (synthesis described in the Supplementary Chemical Procedures) in order to visualize bound proteins by fluorescence. d. Competition of SW208108 with a panel of oxalamide analogues of varying potency. Non-specific band at approximately 40kDa indicates equal sample loading. e. Chemical structures of benzothiazole enantiomers (+)-SW203668 and (–)-SW203668 (H2122 IC_{50} values: 0.029 μM and 0.007 μM, respectively). f. Competition of oxalamide SW208108 with the benzothiazole enantiomers. Non-specific band at approximately 50kDa indicates equal sample loading. g. Correlation of quantified competition to potency of a panel of 30 oxalamide and benzothiazole analogues. Each point represents one replicate. The corresponding gels are shown in figure 1d and supplementary figure 1f.

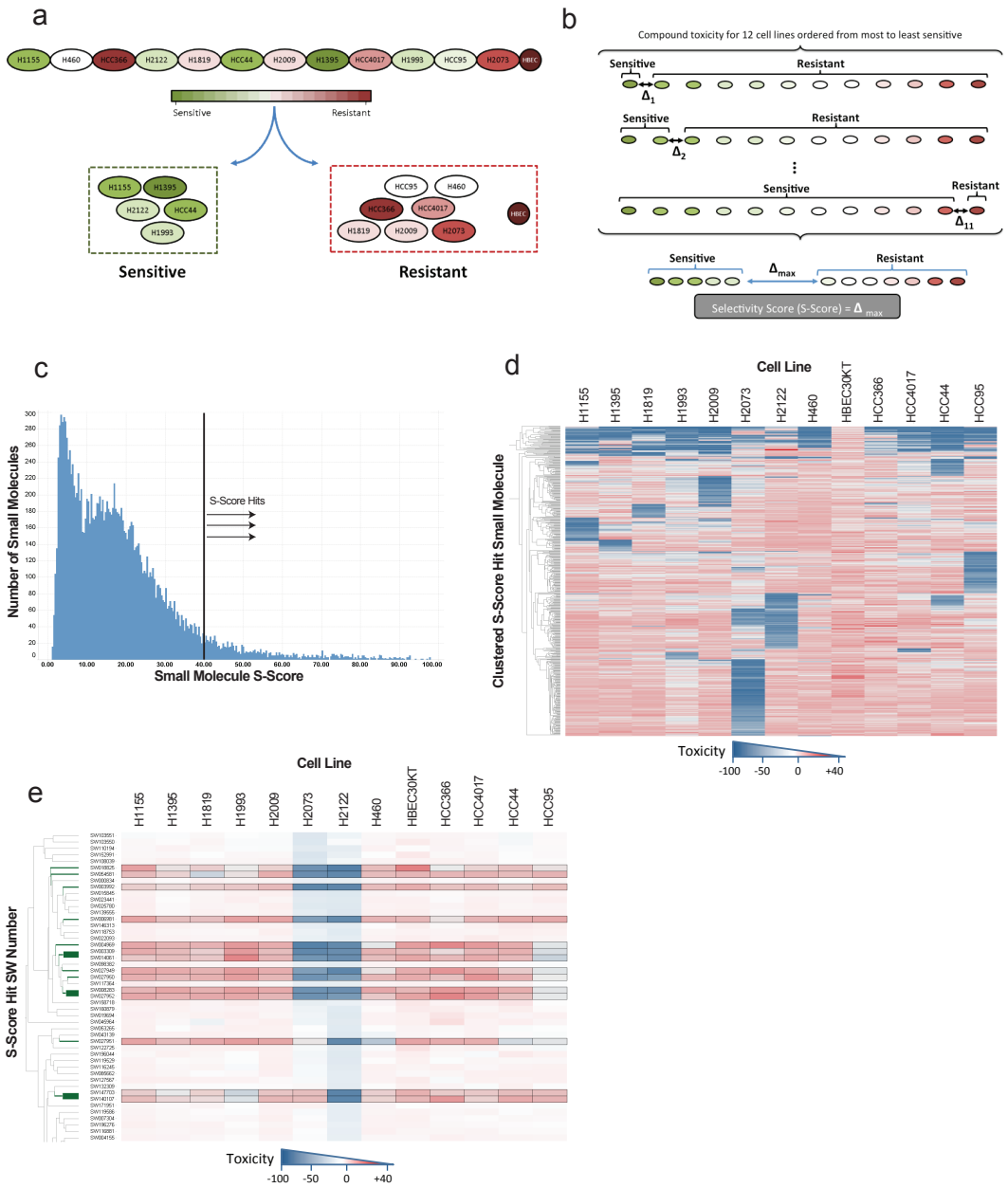

Figure 1-2, part 1

Figure 1-2, part 1: Supporting information for Figure 1-1.

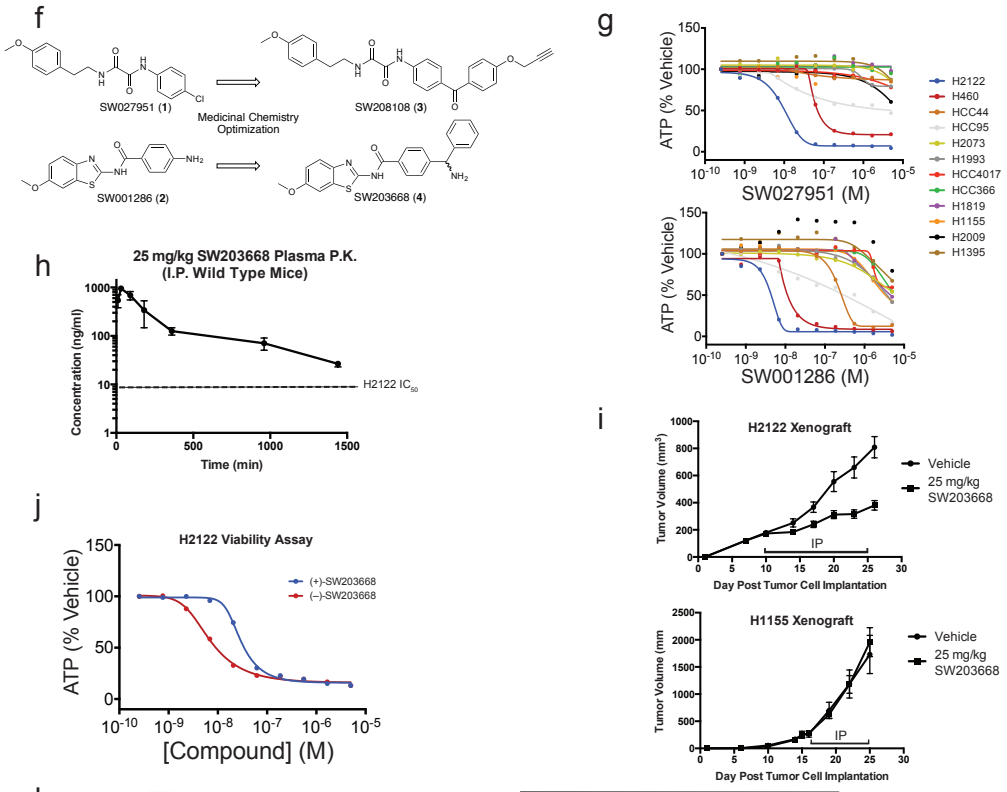

k

	H2122											
	0.1 μM SW208108 + 1 μM of Competitors											
Competitor IC_{50} (μM)	DMSO	0.18	0.009	0.26	0.006	0.04	12.6	0.006	0.04	0.09	0.02	0.004
Lane	1	2	3	4	5	6	7	8	9	10	11	12

	H2122											
	0.1 μM SW208108 + 1 μM of Competitors											
	DMSO	0.07	0.02	0.01	0.04	0.08	0.007	0.5	0.05	11.1	1.8	0.28
	13	14	15	16	17	18	19	20	21	22	23	24

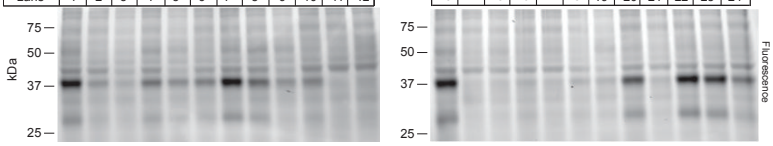

l

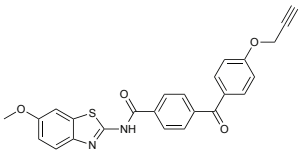

SW209049 (7)
H2122 IC_{50}: 0.29 μM

m

	H2122											
	0.3 μM SW209049 + 3 μM of Competitors											
Compound #	–	2	5	6	23	24	22	26	16	29	31	30
Competitor IC_{50} (μM)	DMSO	0.04	0.03	0.007	0.04	12.6	0.006	0.09	0.04	0.01	0.5	0.08
Lane	1	2	3	4	5	6	7	8	9	10	11	12

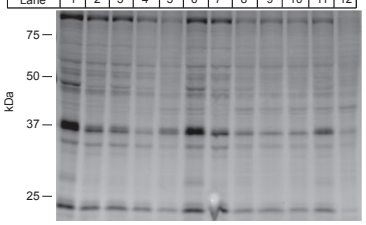

Figure 1-2, part 2

Figure 1-2, part 2: Supporting information for Figure 1-1.

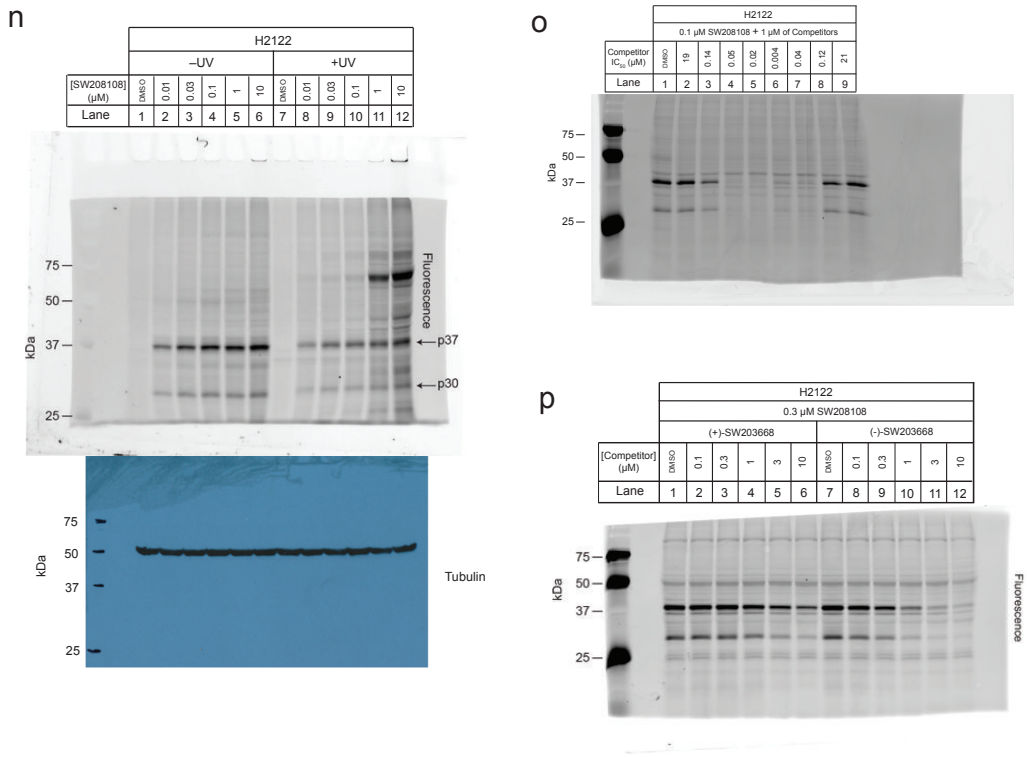

Figure 1-2, part 3

Figure 1-2, part 3: Supporting information for Figure 1-1. See next page for legend.

Legend for Figure 1-2. a. Schematic showing the goal of a high throughput chemical phenotypic screen to identify compounds that were toxic to a subset of NSCLC cell lines but not to immortalized human bronchial epithelial cells, HBEC30KT. b. Schematic showing how the S-Score selectivity metric was calculated. For a given compound, cell lines were ranked based on that compound's toxicity against each line. The differences (Δ_n) of activity between each pair of cell lines were calculated. The S-Score is the maximum difference of activity (Δ_{max}) and allowed identification of sensitive and resistance groups of cell lines. c. Distribution of S-Scores for 15,483 compounds identified as predicted toxins from a high throughput screen of over 200,000 compounds. d. Unsupervised hierarchical clustering of the 520 S-Score hit compounds. e. Zoom in on the heat map to show oxalamide and benzothiazole compounds (highlighted) that are clustering near each other. f. Representative oxalamide and benzothiazole compounds (left) with high S-Scores and optimized versions (right). g. Concentration response curves of library hit oxalamide (top) and benzothiazole (bottom). Each point represents the average of two biological replicates. h. Plasma pharmacokinetics of SW203668 administered at 25 mg/kg by IP injection to wild type (CD-1) mice. Error bars represent standard deviation (n=3 biological replicates). i. Anti-tumor efficacy of benzothiazole, SW203668, in a xenograft model derived from a sensitive cell line, H2122 (top) and an insensitive cell line, H1155 (bottom). Error bars represent standard error of the mean (n=12 biological replicates for H2122 tumors and n=8 for H1155 tumors). j. Concentration response curves for benzothiazole enantiomers in H2122 cells. Each point represents the average of two biological replicates. k. Competition of

SW208108 by a panel of oxalamide and benzothiazole competitors. l. Structure of benzothiazole alkyne UV-activated cross-linker analogue, SW209049. m. Cross-linking of SW209049 in H2122 cells in the absence of UV with and without competitors. n. Full gels for figure 1-1c. o. Full gels for figure 1-1d. p. Full gels for figure 1-1f.

SWID	Structure	Compound #	H2122 IC_{50}	S9 extract half life (min)	MS/MS Transition	*In vivo* PK parameters (10 mg/kg, CD1 mice) Cmax (ng/mL)	AUC (min*ng/mL)	Terminal $T_{1/2}$ (min)
SW202857		20	0.0084	39	389.1 to 209.1	120	14,000	335
SW203668		4	0.03	182	390.1 to 210.1	600	69,000	242
SW208523		11	0.024	138	378.1 to 215.1	260	13,000	36
SW208108		3	0.023	126	457.2 to 135.1	Unable to formulate for in vivo administration > 3 mg/kg		

Table 1: Medicinal chemistry optimization of oxalamides and benzothiazoles

Structure	SWID	Compound #	H2122 IC_{50} (μM)	Relevant to figure:	Lane on gel	p37 Band Intensity	p30 Band Intensity	p37/DMSO	p30/DMSO
	DMSO		-	1d, 1g	1	8974.953	3783.711	1.00	1.00
	208220	12	18.7	1d, 1g	2	8550.347	3040.054	0.95	0.80
	208222	13	0.142	1d, 1g	3	4163.619	1820.326	0.46	0.48
	208522	14	0.0477	1d, 1g	4	96.021	318.849	0.01	0.08
	208523	11	0.0197	1d, 1g	5	190.435	192.607	0.02	0.05
	208458	15	0.00425	1d, 1g	6	950.648	799.698	0.11	0.21
	208459	16	0.0377	1d, 1g	7	655.113	458.92	0.07	0.12
	208393	17	0.115	1d, 1g	8	6497.861	2684.225	0.72	0.71
	208455	18	20.5	1d, 1g	9	9313.882	3105.933	1.04	0.82
	DMSO		-	1g, S1k	1	16419.087	5730.723	1.00	1.00
	206959	19	0.182	1g, S1k	2	3675.782	1326.912	0.22	0.23
	202857	20	0.00923	1g, S1k	3	1918.083	913.134	0.12	0.16
	202864	21	0.256	1g, S1k	4	7632.702	3296.196	0.46	0.58
	208652	22	0.00644	1g, S1k	5	5324.146	1544.912	0.32	0.27
	208653	23	0.0383	1g, S1k	6	6369.924	2250.004	0.39	0.39
	208665	24	12.6	1g, S1k	7	17653.673	6520.693	1.08	1.14
	025780	25	0.00595	1g, S1k	8	9594.459	4641.258	0.58	0.81
	001286	2	0.04	1g, S1k	9	4077.903	1814.933	0.25	0.32
	208401	26	0.09	1g, S1k	10	5488.803	2399.175	0.33	0.42

Table 2, part 1: Quantification of p37 and p30 band intensities in competition assays of small molecules relative to DMSO (intensities were calculated as a percentage of DMSO quantitation from each gel) (continued on next page).

	208523	11	0.0197	1g, S1k	11	1326.205	1177.69	0.08	0.21
	208458	15	0.00425	1g, S1k	12	1450.912	1664.69	0.09	0.29
	DMSO		-	1g, S1k	13	19039.472	7752.894	1.00	1.00
	208562	27	0.0737	1g, S1k	14	702.962	501.255	0.04	0.06
	208117	28	0.0244	1g, S1k	15	900.912	667.648	0.05	0.09
	208456	29	0.0134	1g, S1k	16	2004.397	1517.447	0.11	0.20
	208459	16	0.0377	1g, S1k	17	1810.175	719.548	0.10	0.09
	208561	30	0.0763	1g, S1k	18	2626.296	1306.548	0.14	0.17
	(-)-SW203668	6	0.00666	1g, S1k	19	2431.761	1006.184	0.13	0.13
	206883	31	0.5	1g, S1k	20	14220.309	6414.673	0.75	0.83
	208460	32	0.0456	1g, S1k	21	2867.832	1285.326	0.15	0.17
	208580	33	11.1	1g, S1k	22	20702.501	8290.179	1.09	1.07
	208582	34	1.82	1g, S1k	23	17301.087	7551.986	0.91	0.97
	208412	35	0.277	1g, S1k	24	9750.602	3950.681	0.51	0.51

Table 2, part 2: Quantification of p37 and p30 band intensities in competition assays of small molecules relative to DMSO (intensities were calculated as a percentage of DMSO quantitation from each gel).

Chapter 2: Benzothiazoles and oxalamides bind and inhibit stearoyl CoA desaturase

To purify p37 and p30, we treated H2122 cells with 0.1 μM SW208108 in the presence or absence of an active competitor, and clicked their lysates to a biotin-azide conjugate. We then purified biotin-modified proteins using streptavidin-conjugated beads. We resolved the purified sample by SDS-PAGE, stained with silver and, as expected, it revealed polypeptide bands at approximately 37kDa and 30kDa (Fig. 2-1a). Importantly, we did not recover p37 and p30 when cells were co-exposed to 3 μM of (–)-SW203668 competitor. We excised p37 and p30 as well as corresponding gel slices from the sample that contained the competitor and identified proteins using proteomics. We ranked samples by the ratio of spectral indices between the sample with and without competitor. The highest ratio in both p37 and p30 was acyl CoA desaturase (ACOD), also known as stearoyl CoA desaturase-1 (SCD), with 28 and 13-fold competition, respectively (Supplementary Dataset 3). SCD has a predicted molecular weight of 41 kDa and a known isoform at 30 kDa that is a predicted product of alternative polyadenylation, consistent with the observed molecular weights[26].

To independently confirm that p37 and p30 are SCD, we used either rabbit IgG or SCD antibodies to immunoprecipitate proteins from SW208108-treated cell lysates. After click-mediated conjugation to Alexafluor-532 azide, we detected fluorescent p37 and p30 in the anti-SCD but not rabbit IgG precipitate (Fig. 2-1b).

Next, we demonstrated that a previously reported SCD inhibitor, Abbott-28c, competed with SW208108 for binding to p37 and p30 (Fig 2-1c, d)[27]. Taken together, we concluded that p37 and p30 represent the two known isoforms of SCD.

SCD is a fatty acid desaturase, which introduces a *cis*-double bond in the Δ9 position of fatty acids of varying lengths[14]. *In vitro* assays for SCD activity use fatty acyl CoA substrates tritiated at the Δ9 position[28]. Desaturation at this position by SCD releases tritiated water, which can be counted to determine SCD activity. Using this assay with microsomes derived from H2122 cells, both oxalamides and benzothiazoles inhibited SCD with EC_{50} concentrations of 0.009 and 0.054 μM, respectively (Fig. 2-1e). These values are in the same range as their cytotoxic potencies against sensitive lines. To test whether inhibition of SCD is the cause of toxicity, we tested the efficacy of SW208108 in three different sensitive cell lines in the presence or absence of 100 μM of sodium oleate, a major product of the enzyme. Supplementation of oleate to the media fully rescued three different cancer cell lines from SW208108 toxicity (Fig. 2-1f). We therefore concluded that oxalamides and benzothiazoles covalently bind and inhibit SCD, which leads to cell death through depletion of unsaturated fatty acids.

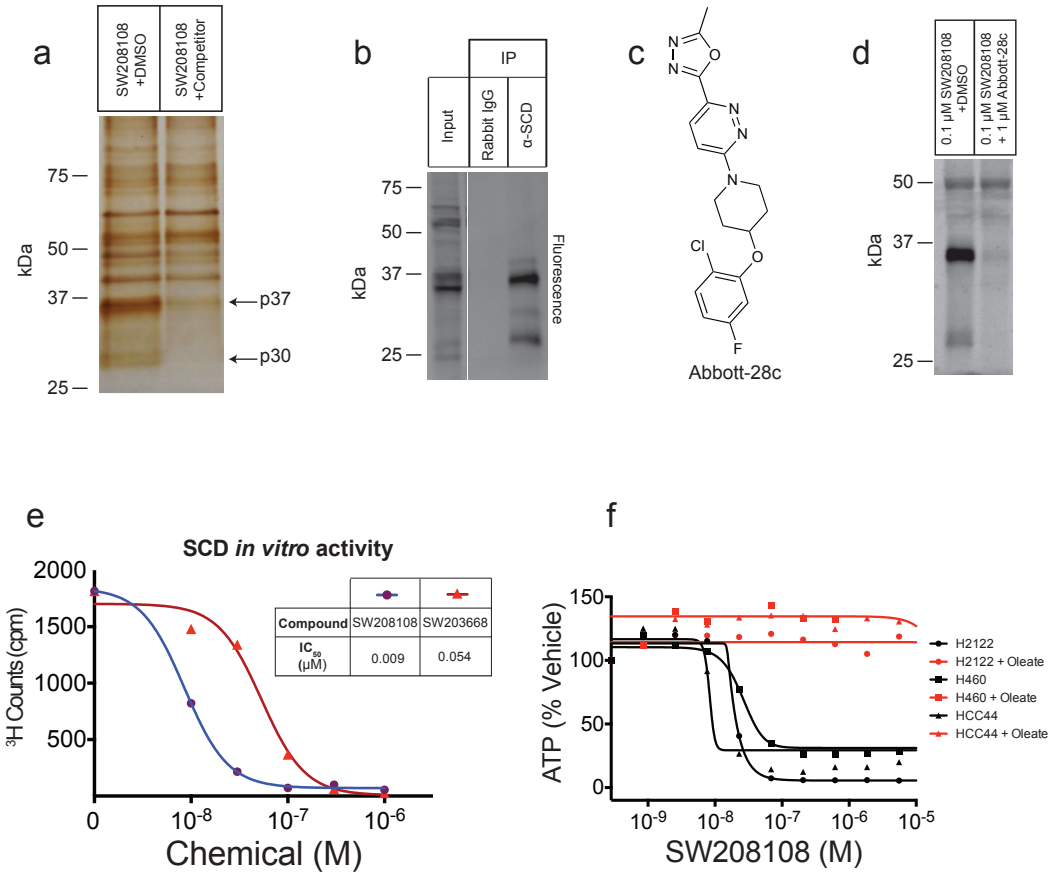

Figure 2-1

Figure 2-1: Stearoyl CoA desaturase-1 (SCD) is the target of the oxalamides and benzothiazoles. (See next page for legend)

Legend for Figure 2-1. a. Silver stain of purified p37 and p30 proteins. H2122 cells were treated with SW208108 with or without 3 μM (–)-SW203668, an active competitor. Full gel image is shown in Supplementary Figure 2a. b. Immunoprecipitation of SCD from 0.1 μM SW208108-treated H2122 cell lysate following conjugation of a fluorescent azide. Full gel is shown in Supplementary Figure 2b. c. Structure of known SCD inhibitor, Abbott-28c. d. Competition of SW208108 with Abbott-28c. Full gel image is shown in Supplementary Figure 2c. e. *In vitro* inhibition of SCD activity by oxalamide and benzothiazole scaffolds in microsomal preparation of H2122 cells. Each data point represents one replicate. Counts shown are after subtraction of counts from a control sample lacking NADPH. f. Rescue of oxalamide toxicity by 100 μM of sodium oleate. Each point represents the average of two biological replicates. Best fit curves of H460 + oleate and HCC44 + oleate are overlapping.

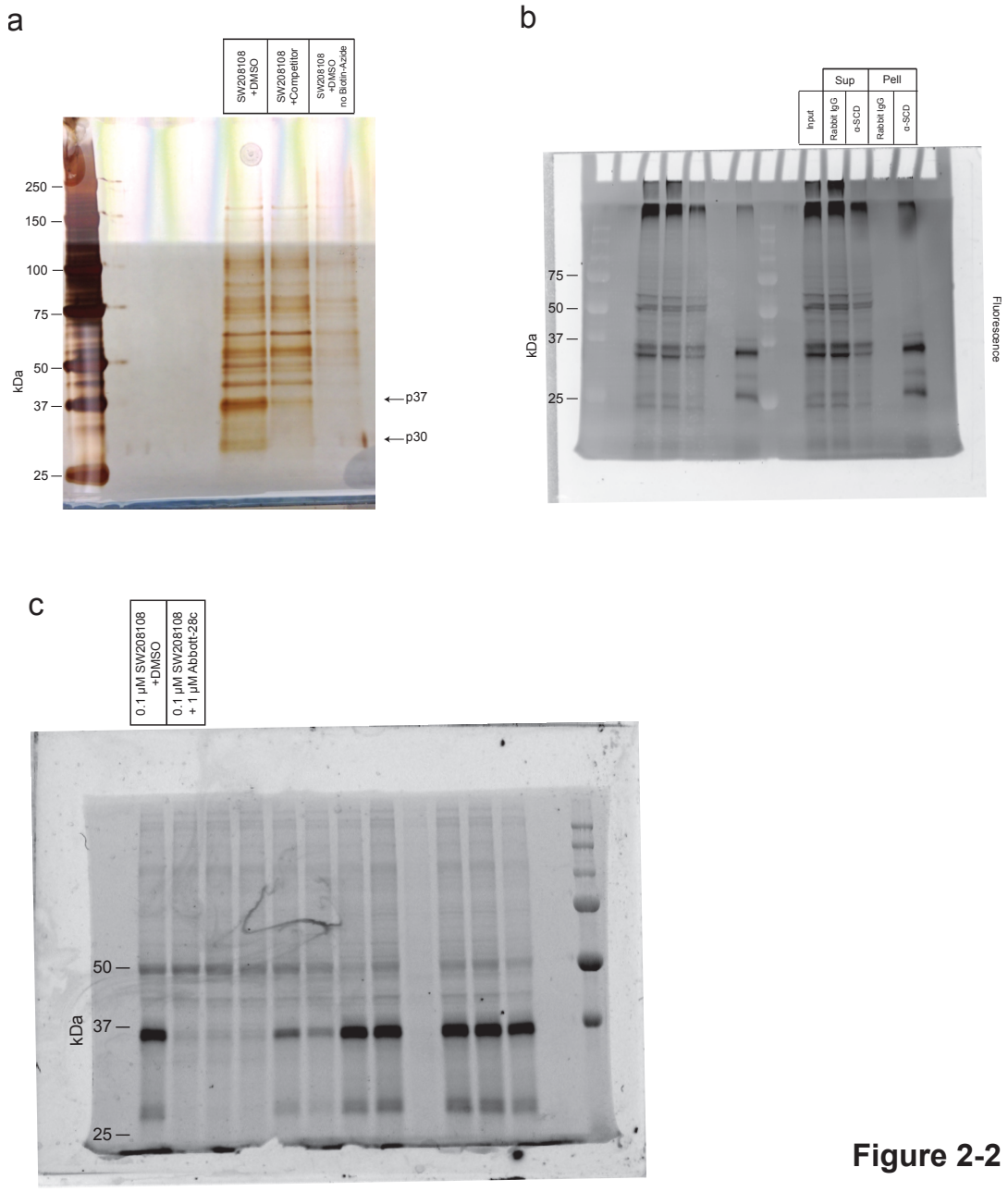

Figure 2-2

Figure 2-2: Supporting information for Figure 2-1. a. Full gel for figure 2-1a. b. Full gel for figure 2-1b. c. Full gel for figure 2-1d.

Chapter 3: Oxalamides covalently bind and inhibit SCD only in sensitive lines

To investigate the mechanism underlying the selectivity of these agents, we compared the oxalamide to Abbott-28c in eight representative cell lines. Unlike SW208108, Abbott-28c was universally toxic to all eight cancer cell lines (IC_{50} range 0.003 to 0.015 μM) (Fig. 3-1a, Fig. 3-2a), indicating that SCD is essential in all cell lines. We discovered that SW208108 is only able to inhibit SCD in a subset of the cancer cell lines. Specifically, we added isotopically labeled palmitic acid ($^{13}C_{16}$-16:0) to the cells, which is elongated to stearic acid ($^{13}C_{16}$-18:0) and then de-saturated to oleic acid by SCD. Both products were expected to maintain the palmitic labeled moiety, thus, the ratio of $^{13}C_{16}$-oleic (18:1) to $^{13}C_{16}$-stearic (18:0) in lipid extracts derived from the cells would reflect SCD activity. In both H2122 and H1155 cell lines, Abbott-28c inhibited SCD in a dose-dependent fashion (Fig. 3-1b). By contrast, SW208108, inhibited SCD only in the sensitive cell line, H2122, but not in the insensitive cell line, H1155. We concluded that SW208108 requires a specific cellular context to inhibit SCD. Indeed, SW208108 bound SCD in the four sensitive cell lines, in the intermediately sensitive cell line (H2073) as well as in one insensitive cell line, H1993 (Fig. 3-1c). In the remaining six insensitive cell lines (including H1155), SW208108 did not bind SCD. The differences in observed SCD binding could not simply be explained by differences in SCD expression (Fig. 3-2b). SCD expression in H1395 and H2009 cells, for example, was nearly as high as in H2122 cells, but there was no evidence of SW208108 binding. We concluded that the ability of SW208108 to bind and inhibit SCD is context dependent and this

feature underpins its selectivity. In the lone outlier, H1993, SW208108 bound p37 and p30 without causing cell death. The nature of this interaction will be discussed later.

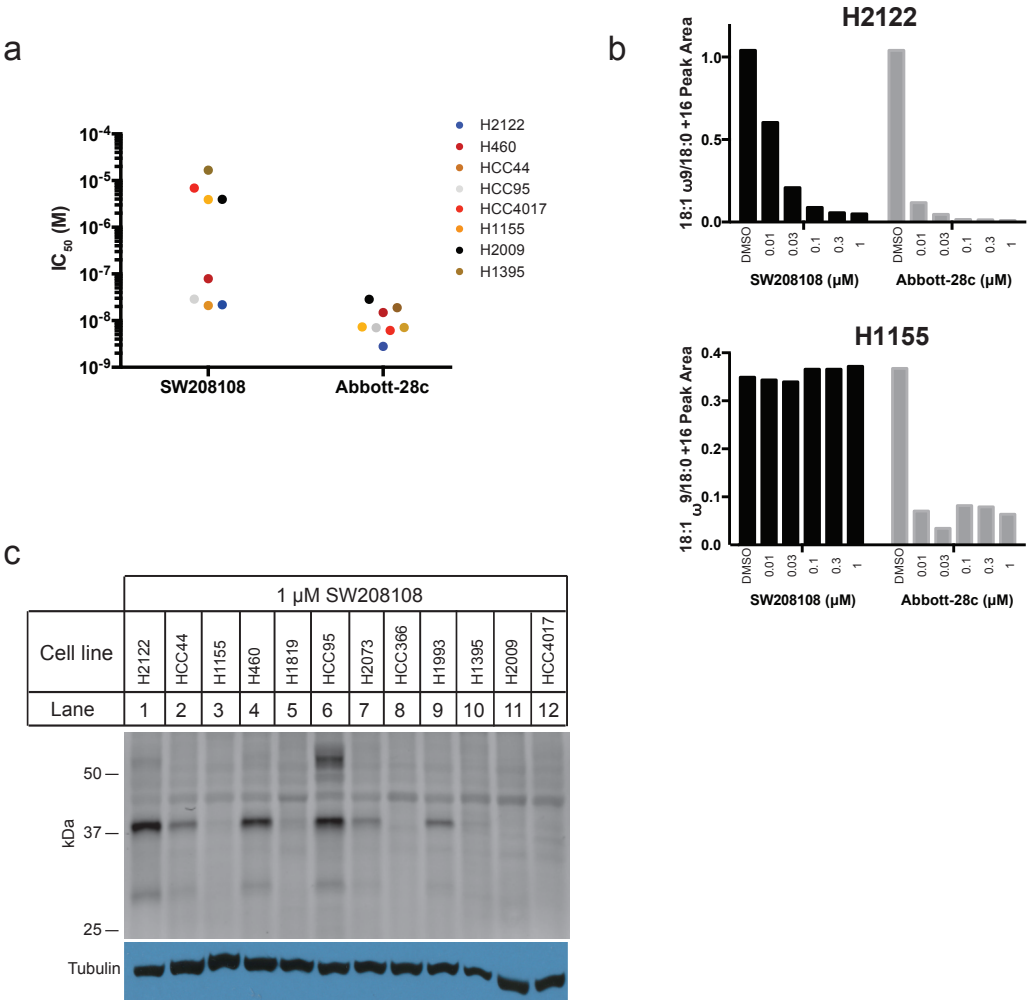

Figure 3-1

Figure 3-1: Known SCD inhibitors are non-selectively toxic to cancer cell lines, while oxalamides are selectively toxic. (See next page for legend).

Legend for Figure 3-1. a. Selectivity of oxalamide SW208108 and a known SCD inhibitor, Abbott-28c, in a panel of eight NSCLC lines. b. Measurements of the conversion of palmitate to oleate, which reflects SCD activity, in the presence of SW208108 or Abbott-28c in H2122 and H1155 cell lines. Each bar represents one replicate. c. Cross-linking of SW208108 in the panel of 12 NSCLC cell lines. Full gel image is shown in Figure 3-2c.

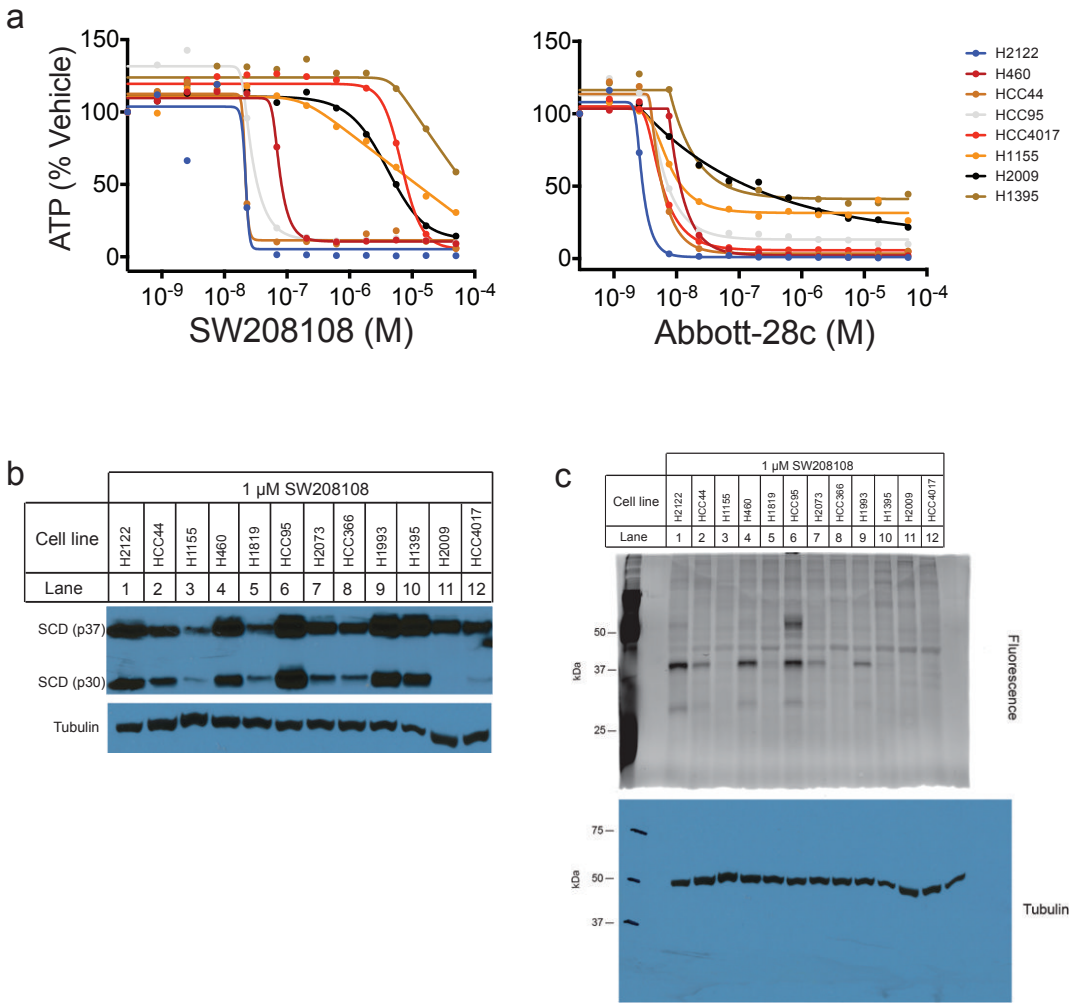

Figure 3-2

Figure 3-2: Supporting information for Figure 3-1. a. Concentration response curves that were used to calculate IC_{50} values for figure 3-1a. Each point represents the average of two biological replicates. b. SCD levels across the panel of 12 NSCLC cell lines using the same samples analyzed in figure 3-1c. The levels of tubulin are reshown to demonstrate equal loading. c. Full gels for figure 3-1c.

Chapter 4: Oxalamides are pro-drugs activated by demethylation

We reasoned that the lack of SW208108 binding to SCD in insensitive cell lines could be a consequence of compound metabolism. We therefore used LC-MS/MS to quantify the levels of SW208108 present in extracts derived from either sensitive (H2122) or insensitive (H1155) cell lines treated with the compound for various times. Surprisingly, we found that the levels of SW208108 decreased by 52% in the presence of H2122 cells after 24 hours, but remained unchanged in the presence of insensitive H1155 cells up to 48 hours (Fig. 4-1a). These results suggested that SW208108 represented a pro-drug and that the observed binding to p37 and p30 resulted from a metabolite that was specifically produced in sensitive cells.

When SW208108 was incubated with H2122 cells, we observed a metabolite that was 14 atomic mass units smaller than the parent drug, consistent with the loss of a methyl group (Fig. 4-2a, b, c). We synthesized authentic samples of dMe-SW208108 (**8**) and determined that the concentration of dMe-SW208108 increased over time in H2122 cells treated with SW208108 but was undetectable at all time points in H1155 (Fig. 4-1b). Of note, the decrease in SW208108 corresponded to a stoichiometric increase in dMe-SW208108, suggesting that it was a major metabolite (Fig. 4-1c). Unlike SW208108, dMe-SW208108 inhibited the conversion of stearate to oleate in both H2122 and H1155 cells (Fig. 4-1d). Concordantly, like Abbott-28c, dMe-SW208108 was universally toxic across the eight sampled cell lines (IC_{50} range 0.003 μM to 0.015 μM) (Fig. 4-1e, Fig. 4-2a). Taken together, we

concluded that the selective toxicity of SW208108 is a consequence of selective metabolism of SW208108 to dMe-SW208108.

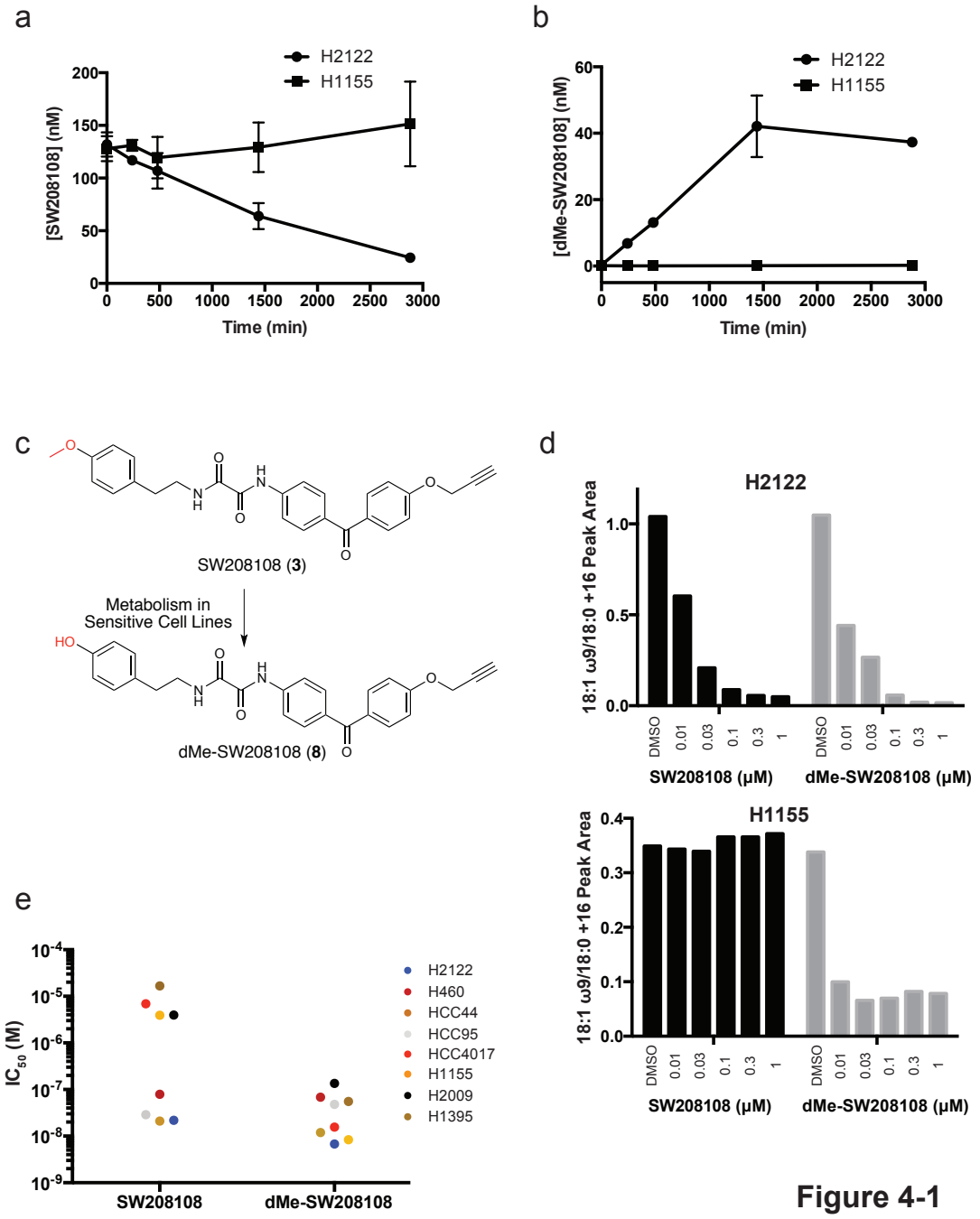

Figure 4-1: Oxalamides inhibit SCD only in sensitive lines. They are pro-drugs that are selectively demethylated in sensitive lines to produce a non-selective SCD inhibitor. (See next page for legend)

Legend for Figure 4-1. a. Levels of SW208108 in the presence of sensitive (H2122) and insensitive (H1155) cell lines. Error bars are plotted for all data points and represent standard deviation (n=3 biological replicates). b. Levels of de-methylated SW208108 (dMe-SW208108) in the above two lines after treatment with SW208108. Error bars represent standard deviation (n=3 biological replicates). c. Metabolism of oxalamide that occurs in the sensitive cell lines. d. Fatty acid flux through SCD in the above two cell lines in the presence of SW208108 or dMe-SW208108. Each bar represents one replicate. Data for SW208108 is re-shown from Fig. 3-1b. e. Selectivity of SW208108 and its demethylated metabolite across a panel of eight cell lines. Data for SW208108 is re-shown from Fig. 3-1a.

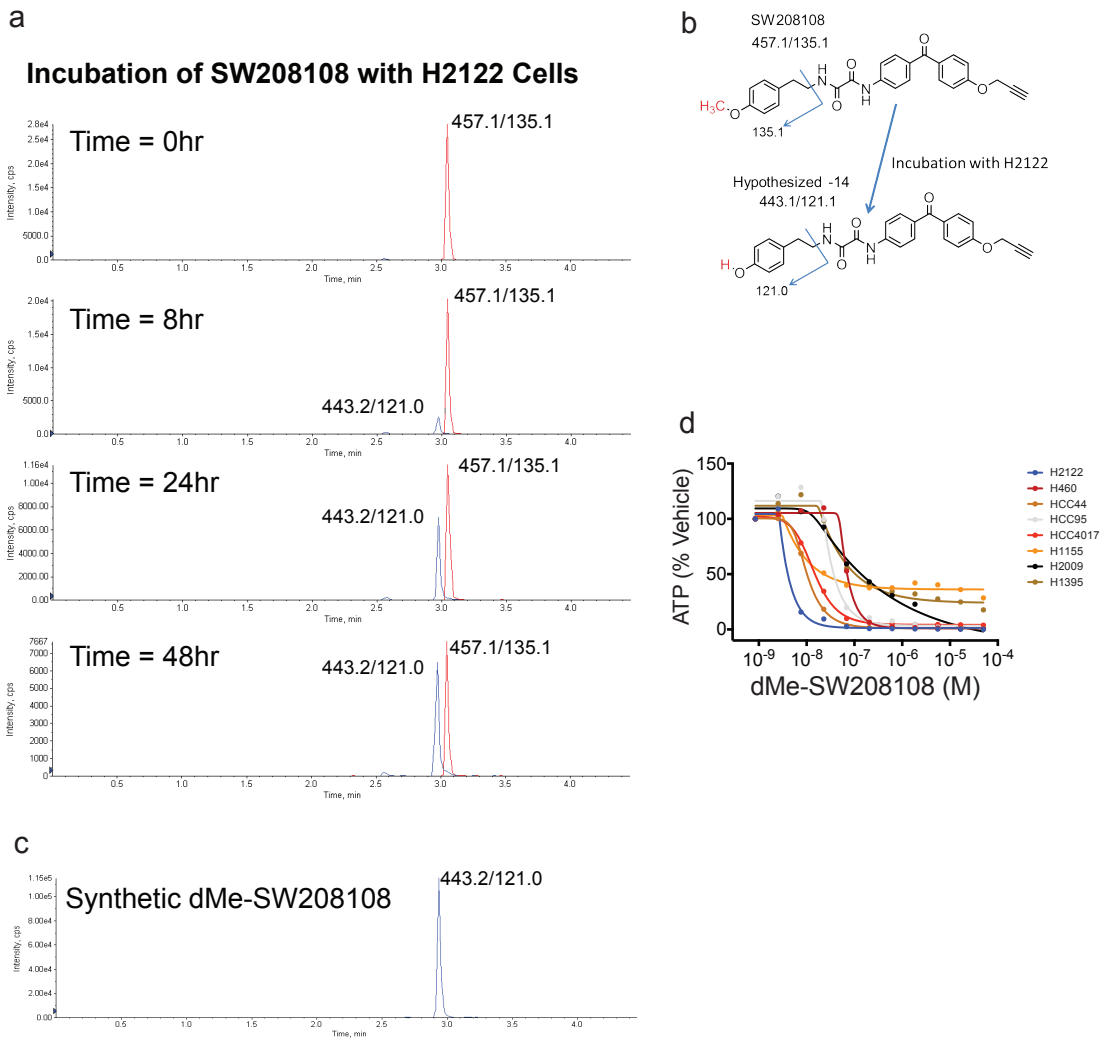

Figure 4-2

Figure 4-2: Supporting information for Figure 4-1. (See next page for legend)

Legend for Figure 4-2. a. LC-MS/MS detection of SW208108 metabolism in the presence of H2122 cells. The peak for SW208108 is shown in red, while the blue peak corresponds to a -14 amu (atomic mass units) metabolite, which increases over time. b. Knowledge of likely metabolic reactions led to prediction of an O-demethylation event. The observed fragmentation pattern of SW208108 in the mass spectrometer was used to predict the likely fragmentation pattern of the O-demethylated metabolite as shown in the schematic. c. LC-MS/MS detection of the synthetic hypothesized de-methylated SW208108 (dMe-SW208108). Its retention time and fragmentation pattern corresponded exactly to the observed metabolite in (a). c. Concentration response curves that were used to calculate IC_{50} values for dMe-SW208108 in Figure 4-1e. Each point represents the average of two biological replicates.

Chapter 5: CYP4F11 activates oxalamides by demethylation

To identify proteins that metabolize SW208108, we focused on proteins of the cytochrome P450 family (CYP). These proteins are frequently expressed in lung epithelial cells and human NSCLC and are known to metabolize and detoxify synthetic compounds[6,29,30]. Using normalized mRNA expression data[31], we compared gene expression of CYP enzymes with the quantified p37 band (Fig. 3-1c), which represents the degree of SCD labeling. CYP isoforms were ranked by how well their expression levels correlated with SCD binding (Table 3). CYP4F11 achieved the highest correlation with an R^2 value of 0.989 (Fig 5-1a). CYP4F11 protein expression across the original panel of 12 cell lines confirmed that it was selectively expressed in the five sensitive lines, but was not expressed in any insensitive lines (Fig. 5-1b).

We used HET0016, a specific inhibitor of Cytochrome P450 4A and 4F enzymes[32], as a tool to test the role of CYP4 family members in oxalamide metabolism. The addition of HET0016 inhibited both the loss of SW208108 and the generation of dMe-SW208108 in H2122 cells (Fig. 5-1c). Furthermore, the addition of HET0016 inhibited the binding of SW208108 to SCD in a dose dependent fashion (Fig. 5-1d). In contrast, HET0016 had no effect on the ability of dMe-SW208108 to bind SCD. Finally, HET0016 rescued the toxicity of SW208108 but not of dMe-SW208108 in H2122 cells (Fig. 5-1e). Taken together, these observations indicated that a CYP4 family member is necessary for SW208108 activation and, therefore, its ability to bind and inhibit SCD.

To test whether CYP4F11 is sufficient for SW208108 to bind SCD, we reconstituted SW208108 binding to SCD in HEK293T cells. HEK293T cells treated with SW208108 demonstrated no evidence of cross-linking to SCD, nor did they show any sign of CYP4F11 expression (Fig 5-1f). Ectopic, transient expression of CYP4F11 produced two weak fluorescent bands, one at 37 kDa and one above 50 kDa, consistent with the endogenous SCD in these cells and the ectopic expression of CYP4F11, respectively (Fig. 5-1f). Consistently, SCD co-expression yielded a more intense p37 band. On the other hand, dMe-SW208108 bound SCD in the absence of CYP4F11. Finally, to test whether CYP4F11 is sufficient for SW208108 toxicity, we ectopically, stably expressed CYP4F11 in H1155 cells, which were otherwise insensitive to SW208108. In H1155 cells that ectopically expressed CYP4F11, SW208108 cross-linked SCD and was toxic (Fig 5-1g, 5h). Based on the above results, we concluded that CYP4F11 de-methylates the oxalamide pro-drug unveiling dMe-SW208108, a covalent, irreversible inhibitor of SCD. Furthermore, the differential expression of CYP4F11 across cell lines explained the selective toxicity observed in our panel of lung cancer cells.

Amongst our panel of 12 cell lines, H1993 was an outlier. We observed that SW208108 cross-linked SCD in H1993 cells (Fig. 3-1c) even though it did not express CYP4F11 (Fig 5-1b) and was not sensitive to SW208108 (Fig 1-1b). One possible explanation is that dMe-SW208108 is generated, but either cannot inhibit SCD in H1993 or SCD is not essential to H1993. However, we found no evidence of either SW208108 metabolism or dMe-SW208108 generation in H1993 cells (Fig. 5-2a). Moreover, dMe-SW208108 was toxic to H1993 cells (IC_{50} = 0.050 μM) (Fig. 5-

2b) demonstrating that SCD is essential in H1993 cells and dMe-SW208108 is active against this cell line. Therefore, we concluded that the cross-linking of SW208108 in H1993 is independent of the CYP4F11-generated metabolite dMe-SW208108. We next assayed binding of other analogues to SCD using our aforementioned competition assay in H1993 cells. Interestingly, we found that unlike in H2122 cells (Fig. 1-2m), the degree of competition did not correlate with analogue IC_{50} (Fig. 5-2c), which suggested a different mode of binding to SCD. We tested whether this mode of binding might represent a mechanism of resistance that prevents productive SCD cross-linking by measuring SW208108 sensitivity in H1993 cells ectopically expressing CYP4F11 (Fig. 5-2d). H1993 cells expressing CYP4F11 were equally sensitive to SW208108 and dMe-SW208108 ruling out a potential resistance mechanism (Fig. 5-2e). Taken together, we concluded that SW208108 unproductively binds SCD in H1993. This binding may be the result of a low abundance metabolite or reflect a contextual difference in SCD. To address the latter possibility, we found no mutations in the expressed *SCD* sequence in H1993 cells, but this does not rule out cell specific post-translational modifications of SCD.

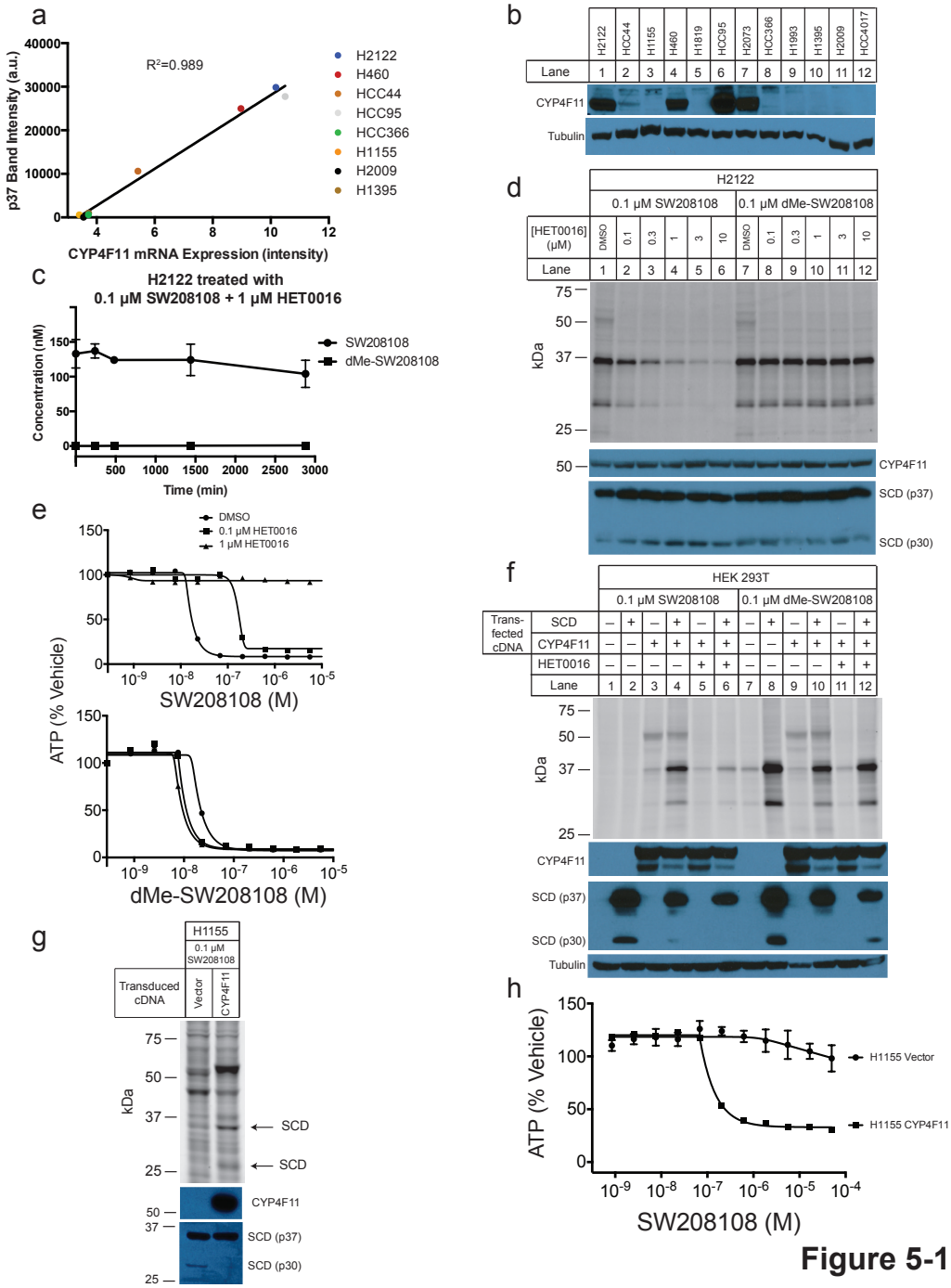

Figure 5-1: Cytochrome P450 4F11 (CYP4F11) is responsible for oxalamide activation in sensitive cell lines and it is not expressed in insensitive cell lines. (See next page for legend)

Legend for Figure 5-1. a. Correlation of CYP4F11 mRNA levels in a panel of eight cell lines to the quantitated intensity of SW208108 cross-linked SCD that is shown in Fig. 3c. b. CYP4F11 levels across the panel of 12 NSCLC lines using the same samples initially shown in figure 3c. Full gel image is shown in Supplementary Figure 5f. The levels of tubulin are also reshown to demonstrate equal loading. c. Effect of a known CYP4F11 inhibitor, HET0016, on SW208108 metabolism in a sensitive line, H2122. Errors represent standard deviation (n=3 biological replicates). d. Inhibition of SW208108 cross-linking to SCD by HET0016. Full gel image is shown in Supplementary Figure 5g. e. HET0016 rescues H2122 cells from toxicity to SW208108 (pro-drug) but not dMe-SW208108 (drug). Each point represents the average of two biological replicates. f. Reconstitution of CYP4F11-dependent SW208108 cross-linking to SCD in HEK293T cells. Full gel image is shown in Supplementary Figure 5h. g. Stable expression of CYP4F11 in an insensitive line, H1155, and resultant cross-linking of SW208108. Full gel image is shown in Supplementary Figure 5i. h. Oxalamide pro-drug, SW208108, concentration response curve of H1155-vector or CYP4F11 infected cell. Each point represents the average of two biological replicates.

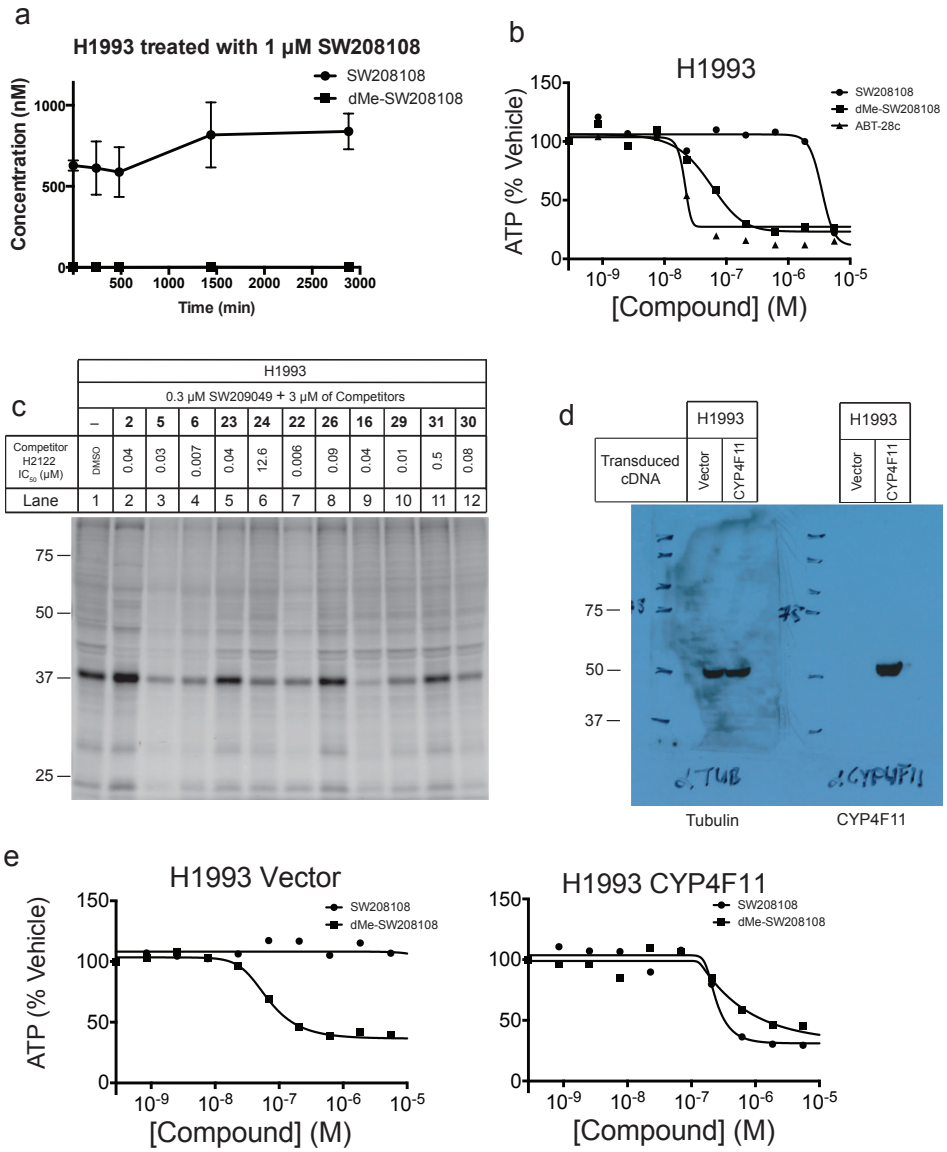

Figure 5-2, part 1

Figure 5-2, part 1. Supporting information for figure 5-1.

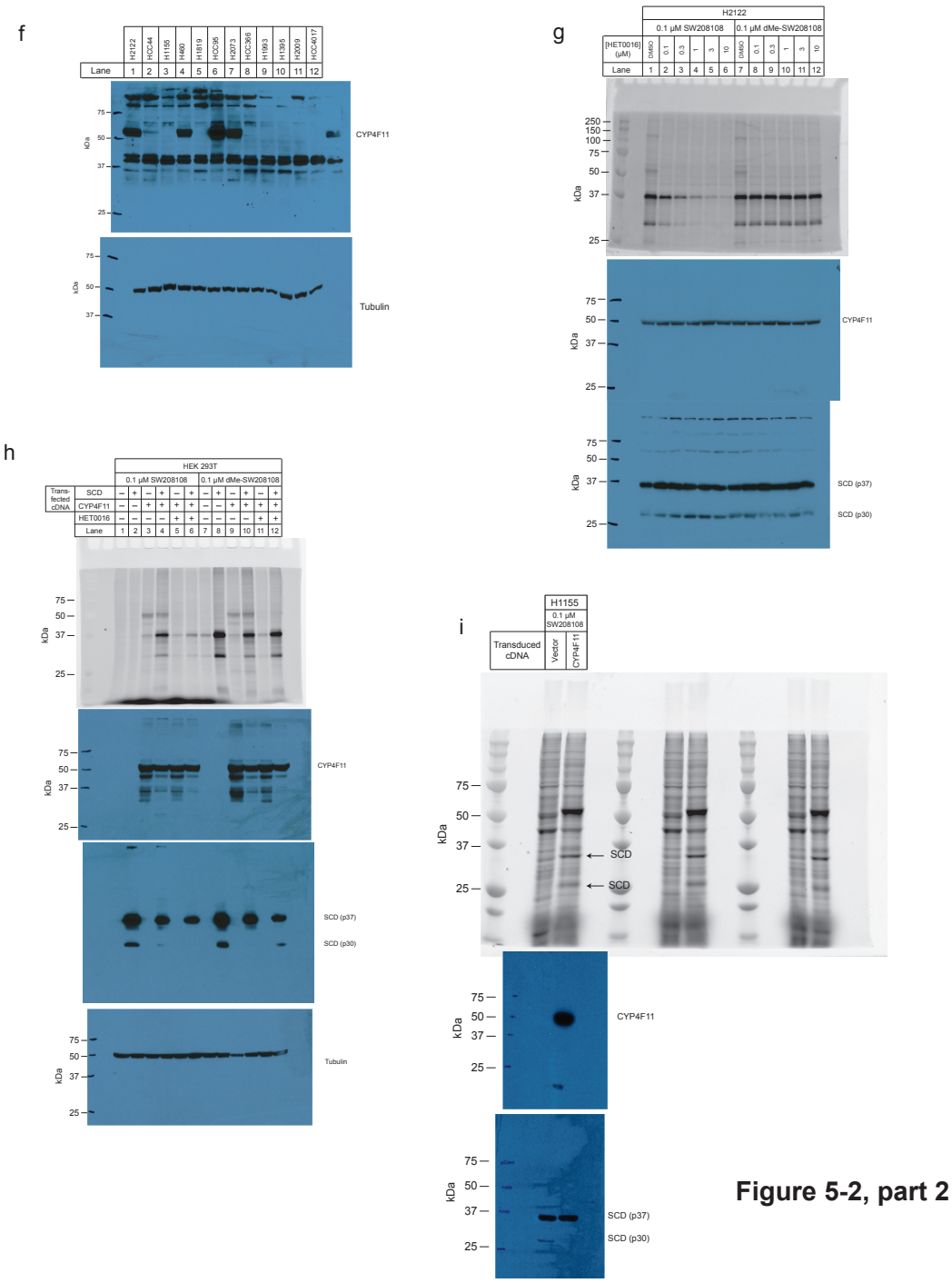

Figure 5-2, part 2

Figure 5-2, part 2. Supporting information for figure 5-2. (See next page for legend)

Legend for Figure 5-2. a. Lack of metabolism of SW208108 in H1993 cells. Errors represent standard deviation (n=3 biological replicates). b. Concentration response of SW208108, dMe-SW208108 and Abbott-28c on H1993 cells. Each point represents the average of two biological replicates. c. Competition of the benzothiazole alkyne SW209049 with a panel of competitors in H1993 cells. d. Western blot of CYP4F11 in H1993 cells transduced with lentivirus containing either a control vector or vector that expresses CYP4F11. Full gel images are shown. e. Concentration response of SW208108 and dMe-SW208108 in H1993 cells transduced with control vector (left) or with CYP4F11 (right). Each point represents the average of two biological replicates. f. Full gels for figure 5-1b. g. Full gels for figure 5-1d. h. Full gels for figure 5-1f. i. Full gels for figure 5-1g.

	NCIH2122_LUNG	NCIH460_LUNG	HCC44_LUNG	HCC95_LUNG	NCIH1395_LUNG	NCIH1155_LUNG	NCIH2009_LUNG	HCC366_LUNG	
p37 intensity	29865.969	24975.07	10602.037	27758.404	996.719	579.284	37.364	612.749	
Gene									**R^2**
CYP4F11	10.18	8.97	5.42	10.50	3.72	3.40	3.55	3.72	0.989
CYP4F2	7.94	4.63	4.24	5.59	4.45	4.11	4.38	3.65	0.577
CYP3A43	3.87	3.79	3.83	3.88	4.06	3.91	3.99	3.94	0.469
CYP2C18	4.32	4.07	4.08	4.04	4.03	3.77	4.01	4.00	0.455
CYP39A1	6.59	6.86	4.55	4.28	4.56	3.94	5.19	4.07	0.399
CYP2C8	3.39	3.43	3.57	3.48	3.70	3.51	4.32	3.61	0.346
CYP7B1	3.79	3.56	3.73	3.79	5.63	3.82	4.58	3.97	0.293
CYP4V2	7.51	5.43	5.03	5.47	5.44	5.84	5.69	4.67	0.244
CYP27A1	5.81	5.91	5.68	5.61	5.87	5.58	6.83	6.83	0.233
CYP26B1	5.69	4.53	5.79	5.38	4.50	4.38	4.49	5.28	0.231
CYP24A1	11.11	4.09	5.43	3.65	3.42	3.73	5.72	3.54	0.225
CYP4F8	4.07	3.90	4.13	4.48	3.95	3.34	3.44	4.38	0.216
CYP1B1-AS1	3.91	3.92	3.56	3.60	3.86	3.31	3.72	3.63	0.196
CYP2S1	4.06	4.34	4.83	6.75	4.13	3.96	4.32	4.51	0.193
CYP2A6	5.81	5.52	6.10	6.01	5.78	5.08	5.32	5.74	0.192
CYP4Z1	3.87	3.55	3.81	3.60	3.30	3.41	3.62	3.75	0.165
CYP26A1	4.35	4.43	4.22	7.65	4.20	4.88	5.00	4.02	0.165
CYP3A5	6.58	4.58	4.46	4.40	5.59	4.18	4.46	4.22	0.164
CYP21A2	5.55	5.31	4.76	4.38	5.16	4.80	4.50	4.53	0.164
CYP4B1	4.01	3.73	3.72	3.93	3.93	3.72	3.89	3.70	0.161
CYP1B1	10.68	10.49	11.11	10.62	11.25	6.16	8.72	10.67	0.159
CYP2A13	6.06	6.19	6.70	6.22	6.35	5.61	5.65	5.71	0.157
CYP4F12	5.11	4.52	4.94	5.09	5.10	4.43	4.27	4.90	0.155
CYP2U1	5.61	5.40	5.02	6.88	6.23	7.81	6.52	6.28	0.145
CYP17A1	3.65	4.27	4.46	3.92	4.38	3.81	4.14	4.11	0.132
CYP20A1	6.67	7.64	7.09	6.50	6.58	7.72	7.88	6.92	0.130
CYP11A1	4.05	3.75	4.35	3.76	8.70	3.85	4.07	3.73	0.115
CYP2C19	4.22	4.46	4.40	4.55	3.94	4.88	5.22	4.57	0.110
CYP2R1	9.28	7.82	8.47	7.28	10.11	7.76	8.52	8.91	0.108
CYP27C1	3.95	3.74	3.97	3.90	3.79	3.85	3.77	6.08	0.093
CYP1A1	5.46	5.15	5.78	6.38	8.22	5.11	6.02	5.76	0.077
CYP4X1	3.73	3.70	3.45	3.62	3.85	3.57	3.44	3.64	0.068
CYP1A2	5.31	5.36	5.74	5.33	5.73	4.83	5.28	4.65	0.066
CYP2J2	6.40	4.27	3.95	4.30	4.74	5.32	5.97	6.59	0.063
CYP3A4	5.33	4.99	5.25	4.93	5.23	4.82	5.13	4.79	0.061
CYP27B1	6.38	6.72	6.18	4.88	9.69	5.53	5.56	5.93	0.050
CYP2W1	3.75	4.10	4.40	4.44	4.06	3.35	3.97	4.29	0.043
CYP11B1	3.72	3.57	3.85	3.69	3.67	3.60	3.67	3.54	0.042
CYP4A11	4.01	4.27	5.38	5.95	5.27	3.96	3.80	4.59	0.041
CYP4F22	3.68	3.72	4.22	4.21	3.78	3.80	3.63	3.86	0.040
CYP7A1	3.83	3.49	3.40	3.33	3.51	3.52	3.67	3.30	0.036
CYP2E1	3.86	4.41	4.02	4.12	3.94	4.05	3.92	5.18	0.035
CYP2B7P1	5.34	5.43	5.52	5.57	5.36	5.48	5.69	5.39	0.032
CYP2A7	4.14	3.61	4.36	3.34	3.97	3.36	3.64	3.35	0.025
CYP4Z2P	3.84	3.75	3.98	4.02	3.54	3.79	4.26	3.55	0.025
CYP19A1	4.41	4.07	4.25	4.00	4.26	4.19	4.45	4.00	0.020
CYP51A1	9.09	9.99	9.14	11.22	10.74	9.45	9.89	9.40	0.020
CYP8B1	4.32	3.86	4.39	4.24	4.39	3.91	4.11	3.98	0.019
CYP2B6	4.15	4.04	4.39	4.52	4.58	3.84	4.56	4.27	0.019
CYP2C9	4.88	4.54	4.46	4.48	4.74	4.37	4.90	4.37	0.015
CYP11B2	4.70	4.74	5.48	4.06	5.61	4.17	4.71	4.01	0.014
CYP46A1	4.10	4.35	4.66	5.32	4.23	3.99	4.09	5.47	0.013
CYP3A7	3.66	3.93	3.59	4.08	3.96	4.01	3.86	3.71	0.000

Table 3: Correlation between p37 band intensity and mRNA expression for members of the CYP family of enzymes

Chapter 6: Oxalamides and benzothiazole pro-drugs spare sebocytes

Efforts to pharmacologically inhibit SCD have been limited by the toxicity of these compounds to sebocytes in the skin and other tissues[20,21]. Given that the methylated oxalamides required activation by CYP4 enzymes in order to bind SCD, we tested whether they inhibited SCD in microsomes prepared from mouse liver and preputial glands. The preputial gland is a specialized sebaceous gland and is used as a tissue source for biochemical studies of sebaceous glands[22]. We found that SW208108 inhibited SCD activity in microsomes derived from liver but not from preputial glands, whereas dMe-SW208108 inhibited SCD in both tissues (Fig. 6-1a). These results suggested that mouse sebocytes do not activate SW208108 *in vitro*.

This tissue-selective inhibition of SCD *in vitro* prompted us to test whether we could spare sebaceous glands *in vivo*. Because the oxalamides were not bioavailable, we first confirmed that the inhibition of SCD by benzothiazoles was also CYP4F11-dependent. Like the oxalamide, we observed that the benzothiazole alkyne SW209049 (**7**) was activated by CYP4F11 in HEK293T cells (Fig. 6-2a). Furthermore, ectopic expression of CYP4F11 in H1155, an SW203668-insensitive cell line, resulted in its sensitization to toxicity by SW203668 (Fig. 6-2b). These results confirmed that CYP4F11 also activates the benzothiazole, SW203668.

We compared SW203668 *in vivo* to a conventional, bioavailable SCD inhibitor developed by Xenon Pharmaceuticals, Xenon compound 45 (**9**)[33] (Fig. 6-2c). Xenon-45 was cytotoxic to H2122 cells (IC_{50} = 0.095 μM) with potency similar to SW203668 (Fig. 6-2d). Further, it exhibited favorable pharmacokinetic properties

at 6 and 20 mg/kg, and its total levels in plasma were comparable to SW203668 in wild type (CD-1) mice (Fig. 6-2e). We dosed CD-1 mice with 20 mg/kg of SW203668 or Xenon-45 once a day for two weeks after which time, skin biopsies were collected. Consistent with prior observations[21], we observed that hair follicles from Xenon-45-treated mice were devoid of sebocytes. In contrast, sebocytes were preserved in SW203668-treated mice and their numbers were significantly higher at 20 mg/kg of SW203668 compared to 20 mg/kg Xenon-45 (Fig. 6-1b, c).

In an initial proof of concept experiment, we compared the anti-tumor efficacy of SW203668 versus the Xenon-45 compound by dosing immune-deficient Nod-Scid mice harboring an H2122 cell-derived tumor xenograft. Administration of 20 mg/kg of SW203668, once daily, inhibited growth of H2122 tumors, while Xenon-45 displayed no efficacy at this dose (Fig. 6-2f). We concluded that SW203668 is less toxic than Xenon-45 and has more efficacy, revealing a wider therapeutic window. Both compounds displayed significantly more sebocyte toxicity in the skin of Nod-Scid tumor-bearing mice than what was seen in wild type mice (6 mg/kg Xenon-45 in Nod-Scid mice versus CD-I mice; p-value = 0.0496, one-tailed t-test, n=3 biological replicates). As a result, in Nod-Scid mice, the SW203668 therapeutic index was evident at a lower dose, 6 mg/kg (Fig. 6-2g). This shift may be attributable to a strain difference.

Finally, we explored whether CYP enzymes other than CYP4F11 are capable of activating the oxalamides and benzothiazoles. We co-expressed SCD and nine different type-4 CYPs in HEK293T cells and evaluated cross-linking of SCD by the oxalamide and benzothiazole pro-drug alkynes, SW208108 and SW209049. Indeed,

several members of the CYP4 family were capable of activating these compounds, including CYP4F11, CYP4F12, CYP4F22 and CYP4V2 (Fig. 6-1d). Based on data from The Cancer Genome Atlas (TCGA)[34], this set of four CYP enzymes is expressed at high levels relative to matched normal tissue in a diverse set of cancers, with each CYP isoform occurring in up to 15% of samples (Fig. 6-1e, Table 4).

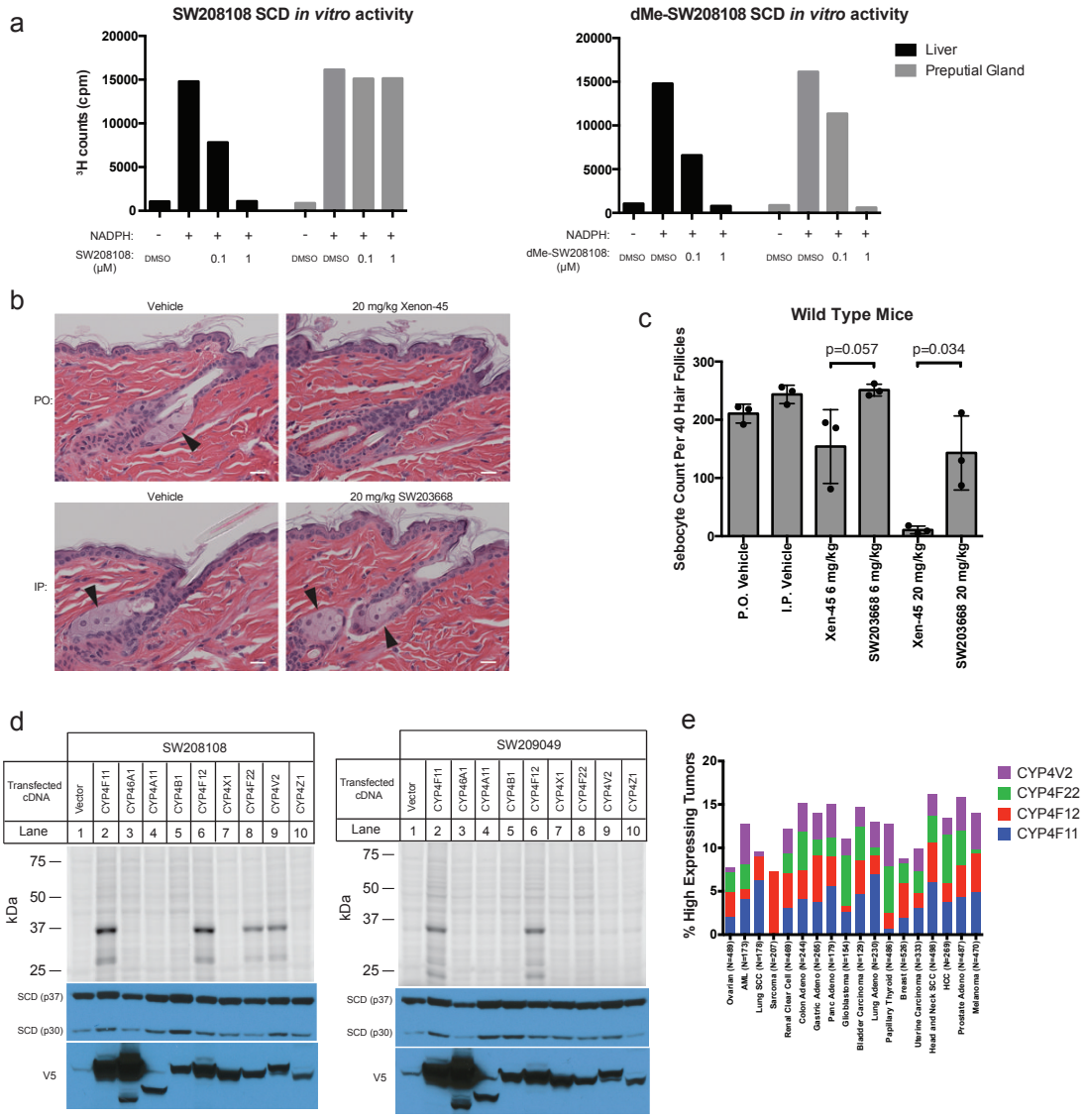

Figure 6-1

Figure 6-1: The CYP-activated SCD inhibitors are not activated by sebaceous glands and display a therapeutic window to avoid sebaceous gland toxicity compared to known SCD inhibitors.

Legend for Figure 6-1. a. *Ex vivo* inhibition of SCD by oxalamide pro-drug SW208108 and active species dMe-SW208108 in wild type mouse liver and sebaceous (preputial) gland microsomes. Each bar represents one replicate. b. Hematoxylin and eosin stained skin sections of wild type mice treated with a known bioavailable SCD inhibitor, Xenon-45, or benzothiazole SW203668 at 20 mg/kg for two weeks, once daily dosing. Arrowheads indicate sebocytes. Scale bars represent 20 μm. c. Quantitation of sebocytes in mouse skin sections of wild type mice treated with 6 or 20 mg/kg for 2 weeks (one-tailed t-test). Error bars represent standard deviation (n=3 biological replicates). d. Oxalamide probe, SW208108, (left) and benzothiazole probe, SW209049, (right) cross-linking in HEK293T cells over-expressing a panel of nine type 4 CYP enzymes. Full gel images are shown in Figure 6-2h. e. Percentage of cancers expressing high levels of the CYP4 family that activate the oxalamides and benzothiazoles. SCC refers to squamous cell carcinoma and HCC refers to hepatocellular carcinoma.

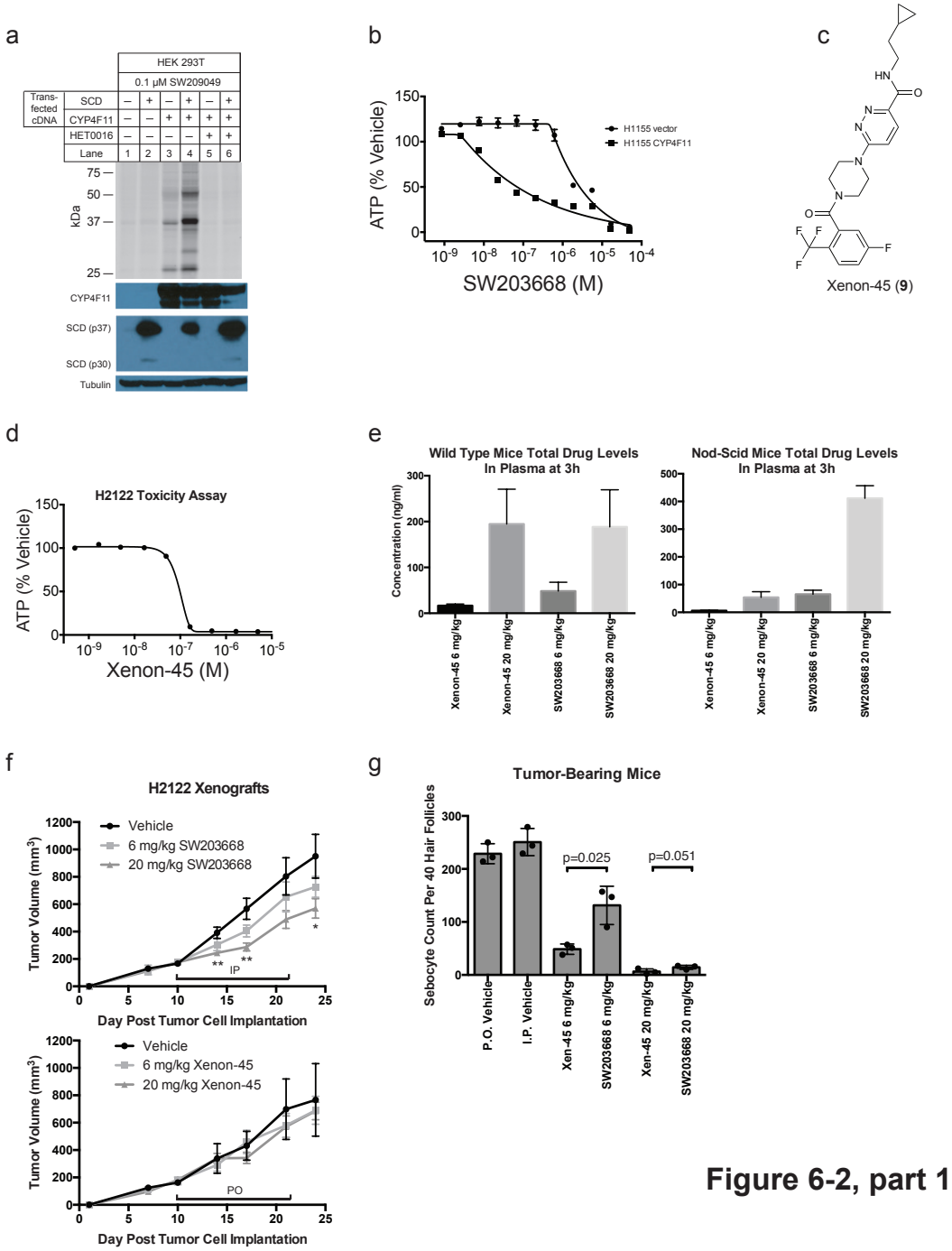

Figure 6-2, part 1

Figure 6-2, part 1: Supporting information for figure 6-1.

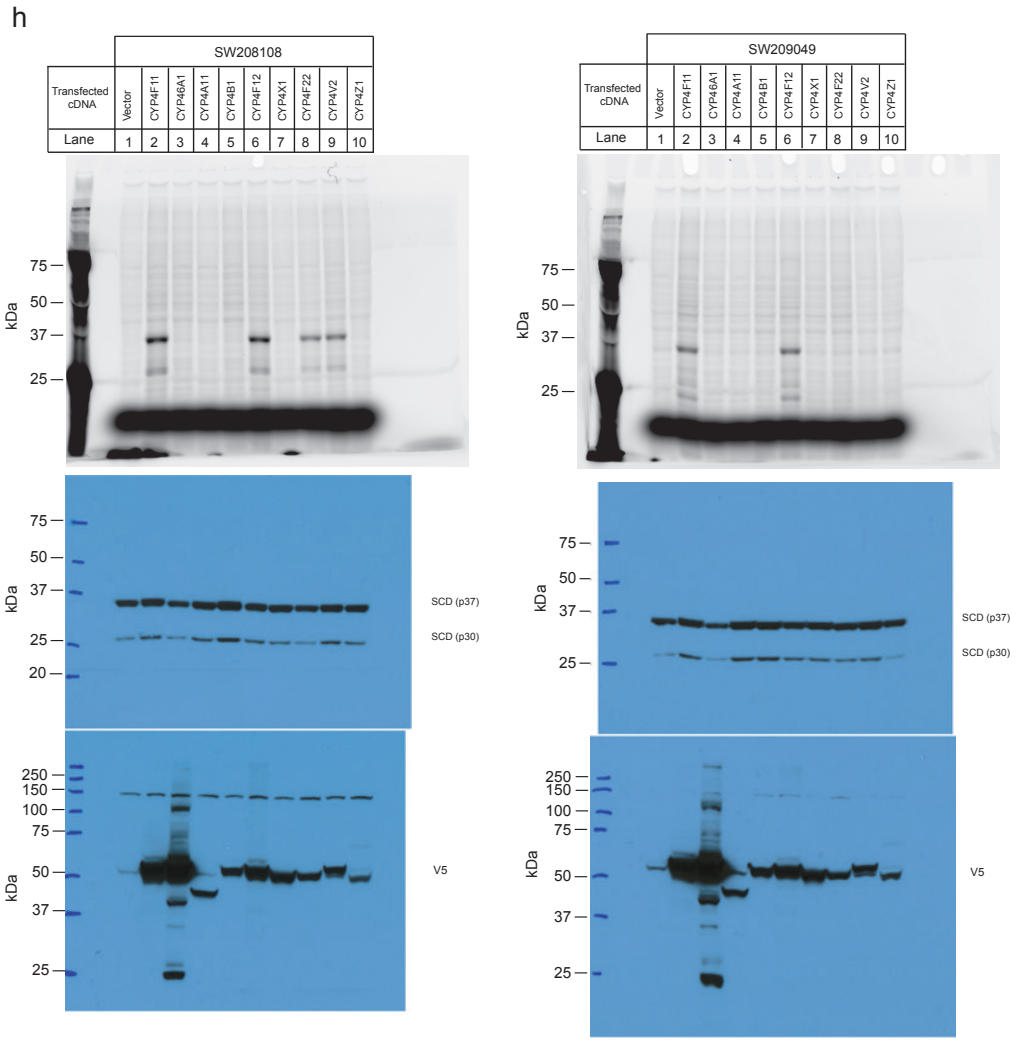

Figure 6-2, part 2

Figure 6-2, part 2: Supplementary information for figure 6-1. (See next page for legend).

Legend for Figure 6-2. a. Reconstitution of cross-linking in HEK293T cells with the benzothiazole probe, SW209049. b. Sensitization of insensitive cell line H1155 to benzothiazole by CYP4F11 expression. Each point represents the average of two biological replicates. c. Structure of Xenon-45 SCD inhibitor. d. Toxicity assay of Xenon-45 in H2122 cells. Each point represents the average of two biological replicates. e. Plasma levels of Xenon-45 and SW203668 after P.O. and I.P. injections, respectively, in wild type (CD-1) mice (left) and Nod-Scid tumor bearing mice (right). Error bars represent standard deviation (n=4 biological replicates). f. Efficacy of benzothiazole, SW203668, (top) and known SCD inhibitor, Xenon-45, (bottom) in a xenograft model of sensitive cell line H2122. Error bars represent standard error of the mean (n=8 biological replicates, except for lower panel vehicle treated mice n=7 where an outlier was removed, see Online Methods). g. Quantitation of sebocytes in skin sections of Nod-Scid tumor-bearing mice treated with 6 or 20 mg/kg of Xenon-45 or SW203668 (one tailed t-test). Error bars represent standard deviation (n=3 biological replicates). h. Full gels for figure 6-1d.

Cancer Type:	Total Samples:	Source:	% CYP4F11 (n)	% CYP4F12 (n)	% CYP4F22 (n)	% CYP4V2 (n)	% CYP46A1 (n)	Total
Ovarian Serous Cystadenocarcinoma	489.00	(TCGA, Nature 2011)	2.04 (10)	2.86 (14)	2.25 (11)	0.61 (3)	2.66 (13)	10.40%
Acute Myeloid Leukemia	173.00	(TCGA, NEJM 2013)	4.05 (7)	1.16 (2)	2.89 (5)	4.62 (8)	4.62 (8)	17.30%
Lung Squamous Cell Carcinoma	178.00	(TCGA, Nature 2012)	6.18 (11)	2.81 (5)	0 (0)	0.56 (1)	5.62 (10)	15.20%
Sarcoma	207.00	(MSKCC/Broad, Nature Genetics 2010)	0 (0)	7.25 (15)	0 (0)	0 (0)	6.28 (13)	13.50%
Kidney Renal Clear Cell Carcinoma	469.00	(TCGA, Nature 2013)	2.99 (14)	4.05 (19)	2.35 (11)	2.77 (13)	2.13 (10)	14.30%
Colorectal Adenocarcinoma	244.00	(TCGA, Nature 2012)	4.1 (10)	3.28 (8)	4.51 (11)	3.28 (8)	1.23 (3)	16.40%
Stomach Adenocarcinoma	265.00	(TCGA, Nature 2014)	3.77 (10)	5.28 (14)	1.89 (5)	3.02 (8)	6.04 (16)	20.00%
Pancreatic Adenocarcinoma	179.00	(TCGA, Provisional)	5.59 (10)	3.35 (6)	2.23 (4)	3.91 (7)	2.23 (4)	17.30%
Glioblastoma	154.00	(TCGA, Cell 2013)	2.6 (4)	0.65 (1)	5.84 (9)	1.95 (3)	3.9 (6)	14.90%
Bladder Urothelial Carcinoma	129.00	(TCGA, Nature 2014)	4.65 (6)	3.88 (5)	3.88 (5)	2.33 (3)	4.65 (6)	19.40%
Lung Adenocarcinoma	230.00	(TCGA, Nature 2014)	6.96 (16)	2.17 (5)	0.87 (2)	3.04 (7)	3.48 (8)	16.50%
Papillary Thyroid Carcinoma	486.00	(TCGA, Cell 2014)	0.62 (3)	1.85 (9)	5.35 (26)	4.94 (24)	4.53 (22)	17.30%
Breast Invasive Carcinoma	526.00	(TCGA, Nature 2012)	1.9 (10)	3.99 (21)	2.28 (12)	0.57 (3)	1.71 (9)	10.50%
Uterine Corpus Endometrioid Carcinoma	333.00	(TCGA, Nature 2013)	3 (10)	1.8 (6)	2.4 (8)	2.7 (9)	6.01 (20)	15.90%
Head and Neck Squamous Cell Carcinoma	498.00	(TCGA, Provisional)	6.02 (30)	4.62 (23)	3.01 (15)	2.61 (13)	3.01 (15)	19.30%
Liver Hepatocellular Carcinoma	269.00	(TCGA, Provisional)	3.72 (10)	2.23 (6)	5.58 (15)	1.86 (5)	1.49 (4)	14.90%
Prostate Adenocarcinoma	487.00	(TCGA, Provisional)	4.31 (21)	3.7 (18)	3.9 (19)	3.9 (19)	2.67 (13)	18.50%
Skin Cutaneous Melanoma	470.00	(TCGA, Provisional)	4.89 (23)	4.47 (21)	0.43 (2)	4.26 (20)	2.13 (10)	16.20%

Table 4: Data collected from cbioportal.org summarizing CYP over-expression in human tumors (figure 6-1e).

Discussion

In this work, we identified a series of oxalamide and benzothiazole compounds as selective toxins to a subset of lung cancer cells. Sensitive cancer cell lines express CYP4F11, which converts these compounds into irreversible SCD inhibitors. Inhibition of SCD in proliferating cancer cells leads to depletion of unsaturated fatty acids (UFAs) and cell death. A balance of saturated fatty acids and UFAs is needed for proper membrane fluidity; therefore, UFAs are necessary for membrane synthesis and hence, cell proliferation[13-15]. Cells can obtain UFA's by *de novo* synthesis from SCD or through uptake from their environment[13]. Given that tumors are nutrient deprived and are likely to have impaired access to exogenous UFAs[13], inhibiting SCD could be a viable strategy for inhibiting tumor growth.

Until now, a major obstacle for targeting SCD in cancer has been the toxicity of systemic SCD inhibitors to sebocytes. Other than this, no other serious toxicity has been identified by whole body inhibition of SCD, either by systemic inhibitors or in mice lacking the major SCD isoform[11,20,35]. We found that our pro-drug SCD inhibitors do not inhibit SCD in sebaceous glands *in vitro*, and that they spare sebaceous glands *in vivo* at doses that significantly inhibit tumor growth.

Interestingly, the canonical SCD inhibitor, Xenon-45, had lower anti-tumor efficacy than the benzothiazoles, even though it exhibited greater skin toxicity and both compounds were cytotoxic to cells in culture at similar concentrations. The site-specific activation of the benzothiazole in the tumor might lead to a concentration effect, whereby the levels of the active compound are higher in the

tumor. Alternatively, the irreversible binding of the benzothiazoles might maintain enzyme inhibition even after the parent compound is cleared from the animal.

In contrast to 4-ipomeanol, which is activated by CYP4B1 into a reactive alkylating agent[7], dMeSW208108 is chemically stable. Based on our SDS-PAGE analysis of cross-linked proteins, with or without UV illumination, we observed a very small number of proteins binding to either the oxalamides or benzothiazoles. Furthermore, oxalamide and benzothiazole toxicity is fully rescued by oleate, even at high concentrations, suggesting that the cytotoxicity is solely due to SCD inhibition.

A major challenge of utilizing CYPs to activate cancer toxins is the concomitant hepatoxicity, because the liver expresses most CYP enzymes. For example, 4-ipomeanol displayed anti-cancer efficacy in pre-clinical models. However, in a phase 1 trial, hepatoxicity was dose limiting in humans[9]. Importantly, SCD inhibition in the liver is not toxic as demonstrated by the mouse liver-specific SCD knockout[11] and the lack of hepatotoxicity in response to SCD inhibitors in mice. In addition, Merck tested a liver-targeted SCD inhibitor in phase 2 clinical trials in patients and did not observe liver toxicity[12]. However, at higher concentrations of the benzothiazole we did observe sebocyte toxicity. One likely explanation is that metabolism of the benzothiazole by the liver leads to increased plasma levels of the active metabolite. In the future, an optimized molecules in which active metabolites are not secreted into the plasma might show an even greater therapeutic index.

Liver-specific targeting of SCD has been the subject of considerable attention for its beneficial metabolic effects. Ntambi and colleagues reported that targeted

deletion of SCD1 in mouse liver resulted in impaired glycogen and glucose synthesis but also prevented carbohydrate induced adiposity and fatty liver[11]. We found that the oxalamides inhibited SCD in liver microsomes. Therefore, liver-specific inhibition of SCD for the treatment of fatty liver disease represents another potential application of these compounds.

Because covalent interactions of oxalamides and benzothiazoles are specific to CYP4F11 and SCD, we hypothesize that there is a shared feature of the SCD and CYP4F11 active sites, which accommodates these molecules and renders them locally reactive. Binding of the oxalamides can be competed away by a known, presumably non-covalent, SCD inhibitor, suggesting that oxalamides bind and react in the active site of SCD. Both SCD and CYP4F11 are iron-containing ER membrane proteins that can hydroxylate fatty acid substrates[36-39]. The similar substrate specificity and chemistry of these two enzymes is likely to be relevant to the activation of our compounds. Recently, two independent groups elucidated the X-ray crystal structure of SCD[40,41]. Co-crystallizing the enzyme in complex with the oxalamides and benzothiazoles could be the subject of a future investigation to shed light on the precise mode of binding of these irreversible SCD inhibitors. Systematic screening of CYPs and other enzymes for the ability to activate oxalamides and benzothiazoles could also be the subject of a future investigation that seeks to define a more comprehensive set of tumor biomarkers for these compounds.

In order to further expand the targetable list of high CYP-expressing cancers, it might be possible to engineer these compounds so that other CYP enzymes activate them. Promega has developed a series of luciferase-based enzyme activity

assays that operate on the same principle as our bioactivatable SCD inhibitors (http://www.promega.com/resources/pubhub/enotes/nonselective-cyp450-assay-using-a-biolum-probe-substrate-that-cross-reacts-with-multiple-p450s/)[42-44]. Luciferin contains a hydroxylated benzothiazole moiety; protection of the hydroxyl as an ether prevents its conversion by luciferase into the luminescent species. CYP enzymes can dealkylate luciferin and the identity of the labile alkyl substituent tunes the specificity to different members of the CYP family, including CYP4 members, such as CYP4F12. The benzothiazole and oxalamide SCD inhibitors might also allow the introduction of diverse alkyl substituents, enabling medicinal chemistry efforts to confer the desired CYP specificity or other pharmacological properties to the parent compound. This principle might also be utilized to expand the therapeutic window of these chemicals. A likely explanation for the sebocyte toxicity we observed is that, at higher doses, the active metabolite is produced by the liver, leaks into the blood stream and reaches the sebaceous glands. One possible strategy to prevent release of the metabolite into the bloodstream would be to alter its specificity to CYP that are not expressed in the liver. Another might be to engineer it such that the active chemical is membrane-impermeable, while the parent is not. In terms of liver-specific targeting of SCD, Merck has developed a series of SCD inhibitors with appended acidic moieties that are substrates for liver anion transporters and are thus retained in the liver[45]. Appending these acidic moieties to the benzothiazole may further increase the therapeutic window for liver targeting. In summary, we present a new principle for pharmacological inhibition of

SCD, which we believe can revive the hope of safely and effectively targeting this enzyme in cancer.

Methods

Experimental Reproducibility. All experiments with the exception of animal experiments were replicated at least twice. Animal experiments used multiple biological replicates determined by a power calculation, which is described in detail in a later section.

High Throughput Screening. See Supplementary Table 1 for a description of assay format and screening procedures.

S-Score Analysis. For the application of the S-score method described in the main text, the activity of each compound against each cell line was expressed as the median of three replicates. The S-score script was implemented in Perl (version 5.22.0) and is shown below:

```
#!/usr/bin/perl -w
open(INS, "input.txt"); open(OUT, ">output.txt"); @a=<INS>; close INS; for ($t=0;
$t<@a; $t++) {chomp $a[$t]; @b=(); @b=split(/   /, $a[$t]); @c=(); @c=sort { $a <=>
$b } @b; $j=0; @delta=(); for ($s=1; $s<@c; $s++) {$delta[$j]=($c[$s]-$c[$s-1]);
$j++;}@d=(); @d=sort { $b <=> $a } @delta; $k=0;for ($ss=0; $ss<@delta; $ss++) {if
($delta[$ss]==$d[0]){$k=$ss; last;}}
$kk=($k+1); print OUT $delta[$k], ""; print OUT $kk, ""; print OUT "\n";} close OUT;
```

Unsupervised, hierarchical clustering. The results from rescreening of the 15,483 compounds which were toxic to at least one of the NSCLC cell lines were clustered using the unsupervised hierarchical clustering algorithm available in Spotfire (version 6.5.3; Tibco, Inc. licensed through Perkin-Elmer, Inc.). The clustering utilized the unweighted pair-group method with arithmetic mean

(UPGMA) and the Euclidean distance measure. Additional details can be found in the manufacturer's user manual and the Perkin-Elmer/Tibco website (http://www.cambridgesoft.com/ensemble/spotfire).

Cell culture and compound concentration responses. All NSCLC cell lines were obtained from the Minna and Gazdar laboratory at UT Southwestern Medical Center. They were screened for mycoplasma and authenticated by short tandem repeat (STR) analysis through the McDermott Core at UT Southwestern. All NSCLC cell lines were cultured in RPMI 1640 (Sigma) supplemented with 5% fetal bovine serum (FBS) (Sigma) and 2mM L-Glutamine (Sigma). HEK293T cells were cultured in DMEM supplemented with 10% FBS and 2 mM L-glutamine. For concentration responses, cells were plated in 96-well plates at 15% confluence in 100 μl of the above media and were allowed to settle overnight. On the next day, this medium was removed and new medium containing a 10-point concentration response was added, starting from 6 μM and decreasing in 3-fold serial dilutions in DMSO. The final concentration of DMSO in each well was 0.5%. Each dose of compound was tested in duplicate and the values displayed represent the average of these duplicates.

Compound Treatment, cell lysis and click chemistry. Cells were plated in 6-well plates at 100,000 cells per well and were allowed to adhere overnight. The next day, the media was replaced with the relevant concentration of compound, diluted from a concentrated DMSO stock 1:1000. All compound treatments were for 2h at 37 °C

and 5% CO_2. For UV cross-linking, cells were placed on ice approximately 3-4 inches below the bulbs in a stratalinker and then exposed to 15 minutes of UVB radiation. The media was removed and the cells were immediately solubilized in 1% SDS, with benzonase (Sigma #E1014) diluted 1:10,000 in Buffer A (50 mM HEPES 7.4, 10 mM KCl, 2 mM $MgCl_2$). Lysates were protein normalized using the BCA assay (Life Technologies #23227) and subjected to a click reaction with 100 μM TBTA (dissolved in 4:1 DMSO:t-butanol), 1 mM TCEP, 2 mM $CuSO_4$ and 25 μM Alexafluor-532 azide **(10)** (see supplementary compound procedures for synthesis) for 1 h at 25°C with agitation. SDS sample buffer was then added to the samples to quench the reaction, and proteins were resolved by SDS-PAGE. A typhoon scanner with a 532 nm excitation laser and a 555 nm emission filter was used to scan the gels for fluorescently labeled proteins.

Purification of compound-bound proteins. Cells were treated with the relevant compounds as described above but on a larger scale, in 15 cm Petri dishes, in order to obtain 100 mg of protein lysate per purification condition. Lysates underwent a click reaction with 100 μM TBTA, 1 mM TCEP, 2 mM $CuSO_4$ and 100 μM diazo biotin azide (Click Chemistry Tools #1041-25) for 1 hour at 25 °C. Proteins were then precipitated with 4 volumes of cold acetone, and the insoluble protein pellets were spun down at 6,000g and resolubilized in 4% SDS and 7M urea in PBS overnight. Insoluble material was collected by centrifugation at 20,000g and lysates were filtered at 0.45 μm and at 0.22 μm. Streptavidin agarose beads (Solu-link #N-1000-010) were then added and incubated with the resolubilized protein for 1 hour at

25 °C. The beads were washed three times with 4% SDS in PBS and the protein was eluted at 95°C in Laemmli sample buffer. Proteins were resolved by SDS-PAGE, and the gel was stained with silver (Pierce #24612). The relevant bands were excised and destained.

Proteomic Analysis. Protein in gel bands were digested overnight with trypsin (Promega) following reduction and alkylation with DTT and iodoacetamide (Sigma). Following solid-phase extraction cleanup with Oasis HLB plates (Waters), the resulting samples were reconstituted in 10 µl of 2% (v/v) acetonitrile (ACN) and 0.1% trifluoroacetic acid in water. 2 µl were injected and analyzed by LC/MS/MS using an Orbitrap Elite mass spectrometer (Thermo Electron) coupled to an Ultimate 3000 RSLC-Nano liquid chromatography system (Dionex). Samples were injected onto a 75µm i.d., 50-cm long Easy Spray column (Thermo) and eluted with a gradient from 1-28% of buffer D in buffer C over 60 min at 250 nl/min flow rate. Buffer C contained 2% (v/v) ACN and 0.1% formic acid in water, and buffer D contained 80% (v/v) ACN, 10% (v/v) trifluoroethanol, and 0.08% formic acid in water. The mass spectrometer operated in positive ion mode with a source voltage of 2.2 kV, capillary temperature of 250°C, and S-lens RF level at 60.0%. MS scans were acquired at 240,000 resolution and up to 14 MS/MS spectra were obtained for each full spectrum acquired using collisionally induced dissociation (CID) for ions with charge ≥2. Raw MS data files were converted to a peak list format and analyzed using the central proteomics facilities pipeline (CPFP), version 2.0.3 [46]. Peptide identification was performed using the X!Tandem[47] and open MS search

algorithm (OMSSA)[48] search engines against the human protein database from Uniprot, with common contaminants and reversed decoy sequences appended[49]. Fragment and precursor tolerances of 20 ppm and 0.5 Da were specified, and three miscleavages were allowed. Carbamidomethylation of Cys was set as a fixed modification and oxidation of Met was set as a variable modification. An additional requirement of two unique peptide sequences per protein was used for protein identification.

Western blots. Proteins were resolved via SDS-PAGE and transferred to 0.5 μm nitrocellulose membranes. Membranes were blocked in 5% milk TBST for 5 minutes and then primary antibodies were added in 5% milk and incubated on a shaker overnight at 4°C. HRP-conjugated antibodies, including secondary antibodies and anti-tubulin-HRP were incubated for 1 hour at room temperature. The following antibodies were used: anti-SCD (1:1000, Pierce #PA5-19682), anti-CYP4F11 (1:500, Santa Cruz, sc-53619), anti-tubulin-HRP (1:10,000, Protein Tech #HRP66031), and anti-V5-HRP (1:5000, Sigma #V2260).

Immunoprecipitation and click chemistry. Protein was extracted with 1% NP-40 Buffer A from SW208108-treated H2122 cells. 1 μg of SCD antibody (Pierce #PA5-19682) or rabbit IgG (Cell Signaling #2729) was added to 500 μg of lysate. Protein-antibody complexes were pulled down with protein A/G beads (Santa Cruz #sc-2003) and were washed with lysis buffer. Buffer A with 1% SDS containing click reagents and the fluorescent dye-azide was added to the beads. After 1 hour, the

beads were spun down and Laemmli buffer was added to the supernatant, which was run on SDS-PAGE and scanned as described above.

SCD *in vitro* assay. We modified previously described procedures[28] in the following way. Reactions were performed in 200 µl with 50 µM of stearoyl [9,10-3H] Coenzyme A (American Radiolabeled Compounds, #ART 0390-50 µCi) in Buffer A. Microsomes were used for all samples and prepared as follows. Cells or tissues were lysed in Buffer A using a syringe or dounce homogenizer, respectively, and centrifuged at 1,000g. The resulting supernatant was centrifuged at 100,000g and the pellet was resuspended in Buffer A yielding the microsomal fraction. For SCD activity assays of H2122, liver and preputial glands, 800, 200 and 1,000 µg of protein were used, respectively. Microsomes were first incubated with the relevant compound at 37°C for 15 minutes with 1 mM NADPH (Sigma #N7505), then stearoyl [9,10-3H] Coenzyme A was added to 50 µM and NADPH was increased to 2 mM. The reactions were allowed to incubate at 37°C for 30 minutes. Then 300 µl cold Buffer A was added and the suspensions were transferred to 100 mg charcoal, mixed briefly. The charcoal was removed by centrifugation at 20,000g. The supernatants were filtered and 200 µl were added to 10 ml of scintillation fluid.

Fatty acid flux analysis. Cells were incubated with 10 µM $^{13}C_{16}$ palmitate (Sigma #605573) for 4 hours at 37 °C. Total fatty acids extracted from approximately 500,000 cells were quantified using GC-ECNI-MS in triplicate as previously described[50]. Basic hydrolysis of lipid extracts was performed as described[51] for the

quantification of pooled free and esterified fatty acids. SCD activity was demonstrated by the quantification of the isotopic m/z ions containing +16 units of mass (from labeled $^{13}C_{16}$-palmitate used as substrate). To avoid misinterpretation due to the excess of remaining $^{13}C_{16}$-palmitate from the cell culture media, we present the flux ratio of ^{13}C labeled oleic to stearic acid.

Expression data. Expression data for the CYP enzymes was obtained from the Cancer Cell Line Encyclopedia (CCLE)[31]. Expression data was available only for eight of the 12 NSCLC cell lines, all of which have been displayed herein.

Plasmids. SCD cDNA was amplified from U2OS cDNA library (5' ATGATGGAATTCCACCGCCatgccggcccacttgctgcagga; 5' ATGATGGGATCCtcagccactcttgtagtttcc) and cloned into pLVX-IRES-Puro (Clontech) using EcoRI and BamHI. CYP4F11 cDNA used in Fig. 5 and Supplementary Fig. S6a was obtained from Open Biosystems (Clone ID: 3846027), was PCR-amplified using the following primers (5' ATGATGTCTAGAATGCCGCAGCTGAGCCTGTCCTGGC; 5' ATGATGGCGGCCGCTCACTGTGAGTTCGCACCCAGGGGCTC) and then cloned into pLVX-IRES-Puro (Clontech) using XbaI and NotI. For Fig. 6d, all CYP cDNAs were obtained from the Invitrogen Ultimate ORF Library Collection in Gateway entry vectors and were cloned into pLX302 (Addgene #25896) using an LR reaction (Life Technologies). In all of the resulting plasmids, the stop codon was mutated to glycine to allow for translation of a short linker followed by a V5 epitope. The primers used for site directed mutagenesis are the following: CYP4A11 (5'

CTCAGGAGGATCAAGGGGGAACCCAGCTTTCTTG and 5'

CAAGAAAGCTGGGTTCCCCCTTGATCCTCCTGAG, CYP4V2 (5'

GAAATGCAGATGAACGCGGGAACCCAGCTTTCTTG and 5'

CAAGAAAGCTGGGTTCCCCCTTGATCCTCCTGAG), CYP4F22 (5'

CTGCCTCCGCGGGCCGGGAACCCAGCTTTCTTG and 5'

CAAGAAAGCTGGGTTCCCGGCCCGCGGAGGCAG), CYP4X1 (5'

GAAACTCTCTGAATGTGGGAACCCAGCTTTCTTG and 5'

CAAGAAAGCTGGGTTCCCACATTCAGAGAGTTTC), CYP4F11 (5'

GTGCGAACTCACAGGGGAACCCAGCTTTCTTG and 5'

CAAGAAAGCTGGGTTCCCCTGTGAGTTCGCAC), CYP4B1 (5'

CTGGGTCTGGGAAGGGGAACCCAGCTTTCTTG and

CAAGAAAGCTGGGTTCCCCTTCCCAGACCCAG), CYP46A1 (5'

CACCACCCCCCTGCGGGAACCCAGCTTTCTTG

and 5' CAAGAAAGCTGGGTTCCCGCAGGGGGGTGGTG), CYP4F12 (5'

GAATGTAAGCTTGCAGGGGAACCCAGCTTTCTTG and 5'

CAAGAAAGCTGGGTTCCCCTGCAAGCTTACATTC), CYP4Z1 (5'

CAAAAAAAGTTTGCGGGAACCCAGCTTTCTTG and 5'

CAAGAAAGCTGGGTTCCCGCAAACTTTTTTTG).

Lentiviral packaging and infection. Lentivirus was generated from pLVX-IRES-Puro and pLVX-IRES-Puro-CYP4F11 by transfecting Lenti-X HEK293T (Clontech) cells with the Fugene HD reagent (Promega #E2312) using the three-vector system,

as decribed[52]. Infections were performed by co-treatment of virus and 8 μg/ml polybrene and after 1d were subjected to 2 μg/ml puromycin selection.

Reconstitution of SCD crosslinking in HEK293T cells. For HEK293T cross-linking reconstitution experiments, 300ng of each plasmid or empty vector was transfected into HEK293T cells in 6-well plates using the Fugene HD reagent (Promega #E2312). Complexes were removed after 5 hours and compound treatments were performed 2 days later. Compound treatments, lysate preparation, western blots and click reactions were then performed as described above.

Animals. Male and female CD-1 mice at 5-7 weeks of age were obtained from Charles River Laboratories (Wilmington, MA). Male and female Nod-Scid mice at 6-8 weeks of age were obtained from the Mouse Breeding Core at UT Southwestern Medical Center. All animal experiments were performed without randomization or blinding. All animal protocols were reviewed by the Institutional Animal Care and Use Committee before studies commenced. The Animal Resource Center at UTSW is accredited by the American Association of Accreditation of Laboratory Animal Care (AAALAC) and follows standards set forth in the Guide for Care and Use of Laboratory Animals. This institution is in full compliance with the Animal Welfare Act.

Analytical LC-MS/MS conditions. SW208108, dMe-SW208108 and SW203668 compound levels for metabolic stability and pharmacokinetic studies were

monitored by LC-MS/MS using an AB Sciex (Framingham, MA) 4000 Qtrap mass spectrometer coupled to a Shimadzu (Columbia, MD) Prominence LC. All three analytes were detected with the mass spectrometer in positive MRM (multiple reaction monitoring) mode by following the precursor to fragment ion transition 457.186 to 135.1 for SW208108, 443.252 to 121.0 for dMe-SW208108 and 390.13 to 210.1 for SW203668. An Agilent C18 XDB column (5 micron, 50 x 4.6 mm) was used for chromatography for all three compounds with the following conditions: Buffer E: dH20 + 0.1% formic acid, Buffer F: methanol + 0.1% formic acid, 0-1.5 min 3% F, 1.5 - 2 min gradient to 100% F, 2 - 3.2 min 100% B, 3.2 - 3.5 min gradient to 3% F, 3.5 - 4.5 3%. N-benzylbenzamide (transition 212.1 to 91.1) or tolbutamide (transition 271.2 t0 91.2) both from Sigma (St. Louis, MO) were used as internal standards (IS).

S9 metabolic stability. For S9 studies, 2 μM of each compound was incubated in a 0.5 ml incubation volume with 0.5 mg (1 mg/ml) of murine CD-1 S9 (combined cytosol and microsome) fractions purchased from Celsis/In Vitro Technologies (Baltimore, MD) and Phase I (an NADPH regenerating system) cofactors (Sigma) for 0-240 min. Reactions were quenched by mixing the incubation mixture with an equal volume of methanol containing formic acid and the N-benzylbenzamide or tolbutamide internal standard. The quenched mixture was vortexed for 15 sec, incubated at room temperature for 10 min and spun for 5 min at 986g. Supernatants were then transferred to an Eppendorf tube and spun in a refrigerated microcentrifuge for 5 min at 16,100g. The second supernatant was transferred to

an HPLC vial and analyzed by LC-MS/MS. Transitions used to monitor compound levels in MRM mode are listed in Supplementary Table 2. Chromatography conditions were similar to those listed for SW203668, dMe-SW203668 and SW208108. Metabolic stability studies using both Phase I and Phase II (UDPGA and PAPS both from Sigma) cofactors were conducted similarly. Metabolism of 7-ethoxycoumarin was used to monitor S9 performance. We used the previously described method[53] with modification for determination of metabolic stability half-life by substrate depletion. A "% remaining" value was used to assess metabolic stability of a compound over time. The LC-MS/MS peak area of the incubated sample at each time point was divided by the LC-MS/MS peak area of the time 0 (T0) sample and multiplied by 100. The natural Log (ln) of the % remaining of compound was then plotted versus time (in min) and a linear regression curve plotted going through the y-intercept at ln(100). The metabolism of some compounds failed to show linear kinetics at later time points, so those time points were excluded. The half-life (T ½) was calculated as T ½ = -0.693/slope. If a negative slope was not observed (no compound loss over time), T ½ is indicated as >240 min, the last time point evaluated.

Determination of compound stability in cell lines. H2122 and H1155 cells were plated at a density of 2,000 cells per well in 96 well plates. After overnight adherence, media was removed and replaced with fresh media containing 100 nM SW208108 +/- the CYP4A and 4F inhibitor, HET0016. The plates were incubated at 37°C, 5% CO_2. At varying times post compound addition, media and cells were lifted

and a two-fold volume of methanol containing 0.2% formic acid and 100 ng/ml of internal standard (N-benzylbenzamide) was added followed by vigorous vortexing and centrifugation at 16,000g for 5 min. The supernatant was analyzed by LC-MS/MS for levels of parent SW208108 and demethylated SW208108 (dMe-SW208108). Compound levels were quantitated in reference to standard curves prepared by adding varying concentrations of SW208108 and synthetic dMe-SW208108 to untreated blank H2122 and H115 lysates and processing as described above.

***In vivo* toxicity studies.** Male 6-week-old CD-1 mice were dosed once daily for 15 days with either SW203668 at 6 and 20 mg/kg intraperitoneal (IP) injection in 10% DMSO, 10% Cremophor EL (Sigma), 80% 50 mM lactic acid, pH 5.5, or Xenon-45 at 6 and 20 mg/kg administered per os (PO), i.e. orally, in 1% carboxymethylcellulose/10% PG/0.1% Tween 20. Male mice were used in order to allow the option of collecting preputial glands for further experiments but they were not utilized in this study. Mice were weighed and visually inspected each day. Three hours after the 15th and last dose, animals were euthanized, blood was collected for evaluation of compound levels, and skin was collected for histological evaluation of compound effects on sebocytes.

Pharmacokinetic studies. Pharmacokinetic studies were performed by injecting 6-7 week old CD-1 female mice with SW203668 at 25 mg/kg IP formulated in 10% DMSO, 10% Cremophor, 80% 50 mM lactic acid, pH 5.5. Female mice were used for

greater ease of maintenance and handling. Animals were sacrificed in groups of three, blood was obtained by cardiac puncture at each time point (0, 10, 30, 90, 180, 360, 960 and 1440 min post dose) using the anticoagulant acidified citrate dextrose, and plasma was isolated by centrifugation. 100 µl of plasma was mixed with 200 µl of methanol containing 0.15% formic acid and 20 ng/ml N-benzylbenzamide IS. The samples were vortexed 15 sec, incubated at room temp for 10' and spun twice at 16,100g at 4^0C in a refrigerated microcentrifuge. The amount of SW203668 present in plasma was quantified by LC-MS/MS to determine the rate of clearance from mouse blood. Standard curves were generated using blank plasma (Bioreclamation, Westbury, NY) spiked with known concentrations of SW203668 and processed as described above. The concentrations of SW203668 in each time-point sample were quantified using Analyst 1.6.1. A value of 3-fold above the signal obtained from blank plasma was designated the limit of detection (LOD). The limit of quantitation (LOQ) was defined as the lowest concentration at which back calculation yielded a concentration within 20% of theoretical. Pharmacokinetic parameters were calculated using the noncompartmental analysis tool of Phoenix WinNonLin (Certara/Pharsight, Sunnyvale, CA). Plasma levels of SW203668 dosed IP daily at 6 and 20 mg/kg and of Xenon-45 dosed PO at 6 and 20 mg/kg in 1% CMC/10% PG/0.1% Tween 20 for 15 days in wild type and tumor bearing Nod-Scid mice were determined similarly.

Xenograft experiments. To determine the group size for xenograft experiments, we defined a response as a 50% reduction in tumor volume in the range of linear

growth of a subcutaneous xenograft (up to ~800 mg). Using a power analysis (Sigma Plot, ANOVA) with an expected difference in tumor volumes of 400 mg (50% of control) and standard deviations in measurements of +/− 200 mg, then a power analysis indicates that a group size of eight will provide 90% power to detect a 50% difference with an alpha of 0.05. Therefore, all xenograft experiments used a group size of at least eight mice. Male and female Nod-Scid mice were injected with 5×10^6 H2122 or H1155 cells by subcutaneous injection in a single site on their left flank. When tumors reached approximately 150-200 mm^3, the animals were randomized into groups of either 12 mice (Supplementary Fig. 1) or 8 mice (Supplementary Fig. 6). In the first experiment, mice bearing either H2122 tumors or H1155 tumors were dosed IP twice daily for 15 days at 25 mg/kg with SW203668 formulated as previously described or with vehicle. In the second experiment, H2122 tumor-bearing mice were dosed once daily with either 6 or 20 mg/kg SW203668 IP or 6 or 20 mg/kg Xenon-45 PO formulated as previously described. Three or seven hours after the final dose, animals were euthanized to evaluate compound levels in plasma and to monitor sebocyte viability. Animals were weighed daily and tumors measured with calipers twice weekly. Tumor volume was calculated according to the formula: Volume = (Length x $Width^2$ x Pi)/6. We used the Grubbs' test ($p<0.0001$) to eliminate one outlier in a mouse harboring a xenograft tumor derived from H2122 cells in Supplementary Fig. 6f (lower panel). Weight loss was less than 15% for twice daily dosing with 25 mg/kg SW203668, up to 7% with once daily Xenon-45 and negligible (<2%) for all other treatment groups.

Tissue harvest and histology preparation. Tissues for routine histology and special stains were harvested from anesthetized mice, were grossly trimmed, and then were immersion fixed in twenty-volumes of 10% neutral-buffered formalin. Following 48-hours of constant agitation in fixative, tissues were briefly rinsed and then dehydrated, cleared, and paraffin embedded by standard procedures[54,55]. Resulting embeds were sectioned on Leica RM2255 rotary microtomes at 5 μm thickness and subsequently stained by routine hematoxylin and eosin. All histology services were performed by members of the Molecular Pathology Core at UT Southwestern.

Microscopy. Review and photography of histologic preparations were carried out on a Leica DM2000 photomicroscope equipped with bright-field illumination. Photomicrography was achieved using this microscope and an Optronics Microfire digital CCD color camera interfaced with Macintosh G4 computer. Images were captured using PictureFrame 2.0 acquisition software (Optronics,Inc. Goleta, CA, USA).

Chemical syntheses (see Supplementary Chemical Procedures document)

References

1 Stratton, M. R., Campbell, P. J. & Futreal, P. A. The cancer genome. *Nature* **458**, 719-724, doi:10.1038/nature07943 (2009).

2 Lynch, T. J. *et al.* Activating mutations in the epidermal growth factor receptor underlying responsiveness of non-small-cell lung cancer to gefitinib. *The New England journal of medicine* **350**, 2129-2139, doi:10.1056/NEJMoa040938 (2004).

3 Kwak, E. L. *et al.* Anaplastic lymphoma kinase inhibition in non-small-cell lung cancer. *The New England journal of medicine* **363**, 1693-1703, doi:10.1056/NEJMoa1006448 (2010).

4 Nguyen, K. S., Neal, J. W. & Wakelee, H. Review of the current targeted therapies for non-small-cell lung cancer. *World journal of clinical oncology* **5**, 576-587, doi:10.5306/wjco.v5.i4.576 (2014).

5 Rodriguez-Antona, C. & Ingelman-Sundberg, M. Cytochrome P450 pharmacogenetics and cancer. *Oncogene* **25**, 1679-1691, doi:10.1038/sj.onc.1209377 (2006).

6 Estabrook, R. W. The remarkable P450s: a historical overview of these versatile hemeprotein catalysts. *FASEB journal : official publication of the Federation of American Societies for Experimental Biology* **10**, 202-204 (1996).

7 Rainov, N. G. *et al.* New prodrug activation gene therapy for cancer using cytochrome P450 4B1 and 2-aminoanthracene/4-ipomeanol. *Human gene therapy* **9**, 1261-1273, doi:10.1089/hum.1998.9.9-1261 (1998).

8 Doloff, J. C. & Waxman, D. J. Adenoviral vectors for prodrug activation-based gene therapy for cancer. *Anti-cancer agents in medicinal chemistry* **14**, 115-126 (2014).

9 Rowinsky, E. K. *et al.* Phase I and pharmacological study of the pulmonary cytotoxin 4-ipomeanol on a single dose schedule in lung cancer patients: hepatotoxicity is dose limiting in humans. *Cancer research* **53**, 1794-1801 (1993).

10 Slaughter, S. R., Statham, C. N., Philpot, R. M. & Boyd, M. R. Covalent binding of metabolites of 4-ipomeanol to rabbit pulmonary and hepatic microsomal proteins and to the enzymes of the pulmonary cytochrome P-450-dependent monooxygenase system. *The Journal of pharmacology and experimental therapeutics* **224**, 252-257 (1983).

11 Miyazaki, M. *et al.* Hepatic stearoyl-CoA desaturase-1 deficiency protects mice from carbohydrate-induced adiposity and hepatic steatosis. *Cell metabolism* **6**, 484-496, doi:10.1016/j.cmet.2007.10.014 (2007).

12 Corp., M. S. D. *Pharmacokinetics and Pharmacodynamics of MK-8245 in Participants With Type 2 Diabetes (MK-8245-012)*, <https://clinicaltrials.gov/ct2/show/results/NCT00972322> (2009).

13 Ackerman, D. & Simon, M. C. Hypoxia, lipids, and cancer: surviving the harsh tumor microenvironment. *Trends in cell biology* **24**, 472-478, doi:10.1016/j.tcb.2014.06.001 (2014).

14 Paton, C. M. & Ntambi, J. M. Biochemical and physiological function of stearoyl-CoA desaturase. *American journal of physiology. Endocrinology and metabolism* **297**, E28-37, doi:10.1152/ajpendo.90897.2008 (2009).
15 Listenberger, L. L. *et al.* Triglyceride accumulation protects against fatty acid-induced lipotoxicity. *Proceedings of the National Academy of Sciences of the United States of America* **100**, 3077-3082, doi:10.1073/pnas.0630588100 (2003).
16 Hess, D., Chisholm, J. W. & Igal, R. A. Inhibition of stearoylCoA desaturase activity blocks cell cycle progression and induces programmed cell death in lung cancer cells. *PloS one* **5**, e11394, doi:10.1371/journal.pone.0011394 (2010).
17 Scaglia, N. & Igal, R. A. Inhibition of Stearoyl-CoA Desaturase 1 expression in human lung adenocarcinoma cells impairs tumorigenesis. *International journal of oncology* **33**, 839-850 (2008).
18 Mason, P. *et al.* SCD1 inhibition causes cancer cell death by depleting mono-unsaturated fatty acids. *PloS one* **7**, e33823, doi:10.1371/journal.pone.0033823 (2012).
19 Roongta, U. V. *et al.* Cancer cell dependence on unsaturated fatty acids implicates stearoyl-CoA desaturase as a target for cancer therapy. *Molecular cancer research : MCR* **9**, 1551-1561, doi:10.1158/1541-7786.MCR-11-0126 (2011).
20 Zhang, Z., Dales, N. A. & Winther, M. D. Opportunities and challenges in developing stearoyl-coenzyme A desaturase-1 inhibitors as novel therapeutics for human disease. *Journal of medicinal chemistry* **57**, 5039-5056, doi:10.1021/jm401516c (2014).
21 Meingassner, J. G. *et al.* Pharmacological inhibition of stearoyl CoA desaturase in the skin induces atrophy of the sebaceous glands. *The Journal of investigative dermatology* **133**, 2091-2094, doi:10.1038/jid.2013.89 (2013).
22 Cheng, J. B. & Russell, D. W. Mammalian wax biosynthesis. II. Expression cloning of wax synthase cDNAs encoding a member of the acyltransferase enzyme family. *The Journal of biological chemistry* **279**, 37798-37807, doi:10.1074/jbc.M406226200 (2004).
23 Kim, H. S. *et al.* Systematic identification of molecular subtype-selective vulnerabilities in non-small-cell lung cancer. *Cell* **155**, 552-566, doi:10.1016/j.cell.2013.09.041 (2013).
24 Ramirez, R. D. *et al.* Immortalization of human bronchial epithelial cells in the absence of viral oncoproteins. *Cancer research* **64**, 9027-9034, doi:10.1158/0008-5472.CAN-04-3703 (2004).
25 Kolb, H. C., Finn, M. G. & Sharpless, K. B. Click Chemistry: Diverse Chemical Function from a Few Good Reactions. *Angewandte Chemie* **40**, 2004-2021 (2001).
26 Zhang, L., Ge, L., Parimoo, S., Stenn, K. & Prouty, S. M. Human stearoyl-CoA desaturase: alternative transcripts generated from a single gene by usage of tandem polyadenylation sites. *The Biochemical journal* **340 (Pt 1)**, 255-264 (1999).

27 Liu, G. *et al.* Discovery of potent, selective, orally bioavailable stearoyl-CoA desaturase 1 inhibitors. *Journal of medicinal chemistry* **50**, 3086-3100, doi:10.1021/jm070219p (2007).
28 Talamo, B. R. & Bloch, K. A new assay for fatty acid desaturation. *Analytical biochemistry* **29**, 300-304 (1969).
29 Hukkanen, J., Pelkonen, O., Hakkola, J. & Raunio, H. Expression and regulation of xenobiotic-metabolizing cytochrome P450 (CYP) enzymes in human lung. *Critical reviews in toxicology* **32**, 391-411, doi:10.1080/20024091064273 (2002).
30 Leclerc, J. *et al.* Profiling gene expression of whole cytochrome P450 superfamily in human bronchial and peripheral lung tissues: Differential expression in non-small cell lung cancers. *Biochimie* **92**, 292-306, doi:10.1016/j.biochi.2009.12.007 (2010).
31 Barretina, J. *et al.* The Cancer Cell Line Encyclopedia enables predictive modelling of anticancer drug sensitivity. *Nature* **483**, 603-607, doi:10.1038/nature11003 (2012).
32 Miyata, N. *et al.* HET0016, a potent and selective inhibitor of 20-HETE synthesizing enzyme. *British journal of pharmacology* **133**, 325-329, doi:10.1038/sj.bjp.0704101 (2001).
33 Zhang, Z. *et al.* Discovery of piperazin-1-ylpyridazine-based potent and selective stearoyl-CoA desaturase-1 inhibitors for the treatment of obesity and metabolic syndrome. *Journal of medicinal chemistry* **56**, 568-583, doi:10.1021/jm301661h (2013).
34 Cerami, E. *et al.* The cBio cancer genomics portal: an open platform for exploring multidimensional cancer genomics data. *Cancer discovery* **2**, 401-404, doi:10.1158/2159-8290.CD-12-0095 (2012).
35 Flowers, M. T., Ade, L., Strable, M. S. & Ntambi, J. M. Combined deletion of SCD1 from adipose tissue and liver does not protect mice from obesity. *Journal of lipid research* **53**, 1646-1653, doi:10.1194/jlr.M027508 (2012).
36 Dhar, M., Sepkovic, D. W., Hirani, V., Magnusson, R. P. & Lasker, J. M. Omega oxidation of 3-hydroxy fatty acids by the human CYP4F gene subfamily enzyme CYP4F11. *Journal of lipid research* **49**, 612-624, doi:10.1194/jlr.M700450-JLR200 (2008).
37 Shanklin, J., Guy, J. E., Mishra, G. & Lindqvist, Y. Desaturases: emerging models for understanding functional diversification of diiron-containing enzymes. *The Journal of biological chemistry* **284**, 18559-18563, doi:10.1074/jbc.R900009200 (2009).
38 Fox, B. G., Lyle, K. S. & Rogge, C. E. Reactions of the diiron enzyme stearoyl-acyl carrier protein desaturase. *Accounts of chemical research* **37**, 421-429, doi:10.1021/ar030186h (2004).
39 Hardwick, J. P. Cytochrome P450 omega hydroxylase (CYP4) function in fatty acid metabolism and metabolic diseases. *Biochemical pharmacology* **75**, 2263-2275, doi:10.1016/j.bcp.2008.03.004 (2008).
40 Wang, H. *et al.* Crystal structure of human stearoyl-coenzyme A desaturase in complex with substrate. *Nature structural & molecular biology* **22**, 581-585, doi:10.1038/nsmb.3049 (2015).

41 Bai, Y. *et al.* X-ray structure of a mammalian stearoyl-CoA desaturase. *Nature*, doi:10.1038/nature14549 (2015).
42 Sobol, M., Ma, D., Unch, J. and Cali, J. J. *Nonselective Cytochrome P450 Enzyme Assay Using a Novel Bioluminescent Probe Substrate that Cross-Reacts with Multiple P450 Enzymes.*, 2008).
43 Sobol, M., Ma, D., Woodroofe, C. C. and Cali, J. J. Cytochrome P450 4F12 Enzyme Assay Using a Novel Bioluminescent Probe Substrate. . (2008).
44 Sobol, M., Ma, D. and Cali, J. J. . Selective Cytochrome P450 4A11 Enzyme Assay Using a Novel Bioluminescent Probe Substrate. (2008).
45 Oballa, R. M. *et al.* Development of a liver-targeted stearoyl-CoA desaturase (SCD) inhibitor (MK-8245) to establish a therapeutic window for the treatment of diabetes and dyslipidemia. *Journal of medicinal chemistry* **54**, 5082-5096, doi:10.1021/jm200319u (2011).
46 Trudgian, D. C. *et al.* CPFP: a central proteomics facilities pipeline. *Bioinformatics* **26**, 1131-1132, doi:10.1093/bioinformatics/btq081 (2010).
47 Craig, R. & Beavis, R. C. TANDEM: matching proteins with tandem mass spectra. *Bioinformatics* **20**, 1466-1467, doi:10.1093/bioinformatics/bth092 (2004).
48 Geer, L. Y. *et al.* Open mass spectrometry search algorithm. *Journal of proteome research* **3**, 958-964, doi:10.1021/pr0499491 (2004).
49 Elias, J. E. & Gygi, S. P. Target-decoy search strategy for increased confidence in large-scale protein identifications by mass spectrometry. *Nature methods* **4**, 207-214, doi:10.1038/nmeth1019 (2007).
50 Quehenberger, O., Armando, A. M. & Dennis, E. A. High sensitivity quantitative lipidomics analysis of fatty acids in biological samples by gas chromatography-mass spectrometry. *Biochimica et biophysica acta* **1811**, 648-656, doi:10.1016/j.bbalip.2011.07.006 (2011).
51 Morselli, E. *et al.* Hypothalamic PGC-1alpha protects against high-fat diet exposure by regulating ERalpha. *Cell reports* **9**, 633-645, doi:10.1016/j.celrep.2014.09.025 (2014).
52 Moffat, J. *et al.* A lentiviral RNAi library for human and mouse genes applied to an arrayed viral high-content screen. *Cell* **124**, 1283-1298, doi:10.1016/j.cell.2006.01.040 (2006).
53 McNaney, C. A. *et al.* An automated liquid chromatography-mass spectrometry process to determine metabolic stability half-life and intrinsic clearance of drug candidates by substrate depletion. *Assay and drug development technologies* **6**, 121-129, doi:10.1089/adt.2007.103 (2008).
54 Shehan, D. C. a. H., B. B. . *Theory and Practice of Histotechnology*. Second edn, (Battelle Press, 1980).
55 Woods, A. E. a. E., R. C. . *Laboratory Histopathology, A Complete Reference*. (Churchill – Livingston Press, 1996).